When did the Indus River of South-Central Asia take on its "modern" drainage configuration?

1   **When did the Indus River take on its "modern" drainage configuration?**

2

3   Yani Najman,[1] Guangsheng Zhuang,[1,2] Andy Carter[3], Lorenzo Gemignani[4,5], Ian Millar[6], Jan Wijbrans[4].

4

5   [1]LEC, Lancaster University, LA1 4YQ, UK

6   [2]Department of Geology and Geophysics, Louisiana State University, Baton Rouge, LA 70803, USA

7   [3] Dept of Earth and Planetary Sciences, Birkbeck College, University of London, UK.

8   [4]Institut für Geologische Wissenschaften, Freie Universität Berlin, D-12249 Berlin, Germany.

9   [5] Department of Earth Sciences, Vrije Universiteit Amsterdam, 1081 HV, Amsterdam, Netherlands

10   [6] NERC Isotope Geosciences Lab, BGS Keyworth, Nottingham, UK.

11

12   **Abstract:**

13   In order for sedimentary archives to be used as a record of hinterland evolution, the factors affecting

14   the archive must be known. In addition to tectonics, a number of factors such as changes in climate and

15   palaeo-drainage, as well as the degree of diagenesis, influence basin sediments. The Indus River-delta-

16   fan system records a history of Himalayan evolution, and both the onshore and offshore sedimentary

17   repositories have been extensively studied to research orogenesis. However, a number of unknowns

18   remain with regards to this system. This paper seeks to elucidate the palaeodrainage of the Indus River,

19   in particular when it took on its modern drainage configuration with respect to conjoinment of the main

20   Himalayan (Punjabi) tributary system with the trunk Indus River. We leverage the fact that the Punjabi

21   tributary system has a significantly different provenance signature to the main trunk Indus, draining

22   mainly the Indian plate. Therefore, after the time when the Punjabi tributary system joined the main

23   trunk Indus, the proportion of Indian plate material in the repositories downstream of the confluence

24   should have a higher proportion of Indian plate material compared to the upstream repository. We

25   compared bulk Sr-Nd data and detrital zircon U-Pb data from the Cenozoic upstream peripheral foreland

26   basin and downstream Indus delta and Indus Fan repositories. We determined that repositories below

27   the confluence had a higher proportion of Indian plate material compared to repositories above the

28   confluence, throughout Neogene times. We therefore conclude that the Indus River took on its current

29   configuration with the Punjabi tributary system draining into the Indus trunk river in the Paleogene,

30   early in the history of the orogen: Pinpointing the exact time when the tributary system joined the Indus

31   should be determinable from a shift to more Indian plate input in the downstream repositories only.

32   Whilst the upstream repository records no change in Indian plate input from Eocene to Neogene times,

33   a shift to increased Indian plate material occurs at the Eocene-Oligocene boundary in the delta but

34   sometime between 50-40 Ma in the fan. Further work is therefore required to understand the

35   discrepancy between the two downstream repositories but nevertheless we can conclude that the

36   tributary system joined the trunk Indus at or before the start of the Oligocene.

37

38   **Keywords**: Himalaya; Indus River; provenance; Sr-Nd analyses, zircon U-Pb analyses, mica Ar-Ar

39   analyses.

40

41   **1.   Introduction**

42   The Himalaya, as the largest orogen on Earth, garners significant interest from researchers in a variety of

43   disciplines. Whilst considerable information on the mountain belt's evolution can be determined from

44   its hard rock geology, its early history is often destroyed in these rocks by later tectonism,

45   metamorphism and/or erosion. In these circumstances, researchers turn to information recorded in the

46   sediment archive of material eroded from the mountain belt and preserved in surrounding sedimentary

47   basins, both onshore and offshore.

48   The main repositories of Himalayan detritus are preserved in the orogen's suture zone , peripheral and

49   axial foreland basins onshore (e.g. Hodges 2000, Najman 2006, Shah 2009), and the Indus and Bengal

50   Fans offshore, which are the world's largest sediment fans (Nyberg et al., 2018). Detritus from all these

51   basins has been studied to document hinterland evolution, using a variety of bulk rock and single grain

52   analytical techniques. For example, studies of the Indus River's sedimentary repository include detrital

53   feldspar Pb isotopic analyses applied to the Indus suture zone molasse (Clift et al., 2001b), detrital zircon

54   fission track and Sm-Nd bulk analyses have been applied to the peripheral foreland basin sedimentary

55   rocks (e.g., Chirouze et al., 2015), detrital zircon U-Pb analyses have been applied to the axial foreland

56   basin (e.g., Zhuang et al., 2015) and heavy mineral and petrography (Andò et al., 2020; Garzanti et al.,

57   2020) data applied to the Indus Fan. However, in order for the sediment archives to be robustly

58   interpreted, a knowledge of the river's palaeo-drainage evolution must be known, since significant

59   drainage changes will affect the sediment archive. Reconstruction of the lower Indus palaeo-drainage is

60   the focus of this paper.

61   Today, the Indus River flows west along the Indus suture zone which separates the Indian and Asian

62   plates, before turning south across the Himalayas to flow eventually into the northern Indian Ocean,

63   giving rise to the Indus Fan (Fig. 1). Here we define the Lower Indus as that part of the Indus River

64   downstream (south) of the Himalayan mountain front, flowing axially, southward along the Indus Basin.

65   We define the Upper Indus as that part of the Indus River which flows through the mountains, sub-

66   divided into the "west-flowing axial Upper Indus" which flows from its headwaters, west, axially along

67   the Indus suture zone, and, further downstream, the "south-flowing transverse Upper Indus", which

68   cuts south across the mountain range (Fig 1A). The main tributaries to the Indus are the Punjabi or

69   Himalayan tributaries of the Jhelum, Chenab, Ravi, Beas and Sutlej Rivers, herein called the Punjabi

70   tributary system, which drain predominantly the Indian plate (Fig 1C).

71   Mid Eocene Owen Ridge sediments are considered to be early Indus Fan material derived from north of

72   the Indian plate (Clift et al., 2001a; Clift et al., 2002a). This places a lower bound on the timing of

73   initiation of the Indus River, although its upstream configuration is debated. For the Upper Indus, the

74   proposed time of its initiation as a river flowing westward along the suture zone ranges from early

75   Eocene through Miocene (Bhattacharya et al., 2020; Clift et al., 2001b; Henderson et al., 2011; Najman,

76   2006; Sinclair and Jaffey, 2001).

77   This paper focusses on the palaeodrainage evolution of the Lower Indus River. Various suggestions have

78   been made regarding whether western Himalayan rivers switched between flowing east to the Ganges

79   and Bengal Fan catchment and west to the Indus River and Fan catchment. Whilst a number of authors

80   based their interpretations on palaeocurrent data from the peripheral foreland basin deposits (e.g. see

81   review in Burbank et al, 1996), Clift and Blusztajn (2005) used geochemical data from the Indus Fan.

82   They considered that changes in the geochemical signature of the Indus Fan sediment archive after 5 Ma

83   represented a major drainage change in the Lower Indus at this time, when the Punjab tributaries to the

84   Lower Indus River (Jhelum, Chenab, Ravi and Sutlej Rivers, Figs. 1A and 1C) switched from flowing east

85   to the Ganges and Bengal Fan, to west to the Indus River and Indus Fan. However, Chirouze et al. (2015),

86   considered that this geochemical change could be better interpreted as the result of variations in upland

87   exhumation. This suggestion was later agreed upon by the original proponents of the drainage diversion

88   hypothesis (Clift et al. (2019) and Zhou et al. (2021)) and thus the timing when the Indus River took on

89   its current configuration with respect to the Punjab tributary system remains unknown.

90   Using a similar rationale to Chirouze et al (2015), we compare provenance indicators from upstream and

91   downstream of the confluence of the Punjab tributary system with the Indus River, and from this

92   comparison we determine when a provenance change in the downstream repository is detected and

93   thus when the tributary system joined the trunk Indus. We extend the peripheral foreland basin Sr-Nd

94   dataset of Chirouze et al (2015) from the mid Miocene, down section as far as the Eocene in order to

95   determine when the provenance change occurred, and additionally we apply new provenance

96   indicators, namely detrital zircon U-Pb ages and detrital white mica Ar-Ar ages.

97

98   **2.   Background:**

99   ***2.1 Himalayan geology***

100   *2.1.1 Tectonic units*

101   The Indus suture zone separates the Asian Lhasa Terrane to the north from the Indian plate to the

102   south. In the west, the Kohistan-Ladakh intra-oceanic island arc (KLIA) is sandwiched between the

103   Indian and Asian plates, with the southern margin of the Asian plate at this location comprised of the

104   Karakoram and Hindu Kush). The northern suture separating the Asian plate and KLIA is termed the

105   Shyok Suture Zone and the southern suture separating the KLIA and Indian plate is termed the Indus

106   Suture zone, also known as the Main Mantle Thrust in this region (Fig. 1C). The Indus River flows west

107   along the Indus suture zone before turning south to cross the Himalaya and foreland basin before

108   debouching into the Arabian Sea.

109   The Lhasa terrane comprises Phanerozoic low grade metamorphic and sedimentary cover overlying

110   Precambrian-Cambrian basement (e.g., Leier et al., 2007). Along its southern rampart are intruded the

111   Gangdese continental arc batholiths of the Transhimalaya which represent the Andean-type southern

112   margin of Asia prior to consumption of the intervening Neo-Tethys ocean (Schärer et al., 1984). Whilst

113   Gangdese intrusions are Mesozoic-Paleogene aged, post-collisional igneous activity continued into

114   Miocene times (Hodges, 2000). To the west, the Lhasa terrane terminates against the Karakoram Fault.

115   West of the fault, the southern margin of Asia is represented by the Karakoram (Fig 1C). The Karakoram

116   terrane is divided into three units (Hildebrand et al., 1998; Hildebrand et al., 2001; Searle et al., 1999):

117   the Northern Karakoram Sedimentary Unit, the Southern Karakoram Metamorphic Belt and the

118   intervening Karakoram Batholith. The Northern Karakoram Sedimentary Unit comprises pre-Ordovician

119   crystalline basement covered by an Ordovician to Cretaceous sedimentary succession (Gaetani and

120   Garzanti, 1991; Gaetani et al., 1993; Zanchi and Gaetani, 2011). The Karakoram Batholith includes pre-

121   India–Asia collision, Andean-type subduction-related granitoids and post-India–Asia collision

122   leucogranites. Age of metamorphism of the Southern Karakoram Metamorphic Belt ranges from Late

123   Cretaceous to late Miocene (Fraser et al., 2001; Palin et al., 2012; Searle et al., 2010).

124   The Kohistan-Ladakh Island arc (KLIA) separates the Indian and Asian plates in the west of the orogen. It

125   consists of Late Cretaceous and Eocene plutonic belts, and pyroxene granulites, calc-alkaline volcanics,

126   amphibolites, and minor metasediments (Coward et al., 1984; Schaltegger et al., 2002), fringed by

127   ophiolitic melange in the southern suture (DiPietro et al., 2000; DiPietro and Pogue, 2004).

128   The Indian plate lies to the south of the KLIA. As summarised in Hodges (2000), In the central and

129   eastern part of the orogen, the Indian plate Himalaya is divided, from north to south, into the Tethyan

130   Himalaya, the Greater Himalaya, Lesser Himalaya and Cenozoic foreland basin sedimentary rocks of the

131   Sub-Himalaya (Fig 1C). Typically, the Tethyan Himalaya, separated from the Greater Himalaya to the

132   south by the South Tibetan Detachment System, consists of Paleozoic–Mesozoic sedimentary and low-

133   grade metasedimentary rocks which were deposited on the Tethyan ocean passive margin; the Greater

134   Himalaya, separated from the Lesser Himalaya to the south by the Main Central Thrust, consists

135   predominantly of medium- to high-grade Neoproterozoic-Ordovician metamorphic rocks that were

136   subjected to metamorphism and anatexis during the Cenozoic Himalayan orogeny when they were

137   intruded by Neogene leucogranites; and the Lesser Himalaya, separated from the Cenozoic Sub-

138   Himalaya foreland basin sedimentary rocks to the south by the Main Boundary Thrust, consisting of

139   Paleoproterozoic metamorphosed and unmetamorphosed Indian plate rocks. These lithologies also

140   broadly constitute the Indian plate Himalaya to the west in Pakistan. However, exact correlation is

141   uncertain, the degree of metamorphism differs, and the lithologies are not structurally imbricated in the

142   same way (Treloar et al., 2019). According to DiPietro and Pogue (2004), north of the Khairabad Thrust

143   (MCT equivalent in Pakistan) metamorphosed rocks of ages equivalent to the Tethyan, Greater and

144   Lesser Himalaya are found, whilst both Lesser and Tethyan equivalents are found between the

145   Khairabad Thrust and the MBT. The Nanga Parbat syntaxis is considered to be of Lesser, Greater and

146   Tethyan Himalayan affinity (Argles et al., 2003).   In this paper, we refer to the Neoproterozoic-

147   Ordovician rocks as *Greater Himalayan lithological correlatives*, the Paleoproterozoic rocks as *Lesser*

148   *Himalayan lithological correlatives*, and the Paleozoic-Mesozoic rocks as *Tethyan Himalaya lithological*

149   *correlatives*. Such terms do not reflect the location of the rocks within the various thrust-bound

150   terranes, as they do further east.

151   The units described above have distinct zircon U-Pb ages and Nd isotope signatures associated with

152   different crustal evolution histories (e.g., Argles et al., 2003; Clift et al., 2019; DeCelles et al., 2004;

153   DeCelles et al., 2016a; Gehrels et al., 2011; Najman, 2006). These differences, (Table 1), allow for use of

154   these techniques as provenance indicators in the detrital record downstream (e.g., Clift et al., 2019;

155   DeCelles et al., 2004; DeCelles et al., 2016a; Gehrels et al., 2011; Najman, 2006).

156   The overwhelming majority of zircons from the Indian plate have U-Pb ages >400 Ma (DeCelles et al.,

157   2004; Gehrels et al., 2011), with the minor exception of grains dated ~130 Ma from the Tethyan

158   Himalaya (e.g. Clift et al., 2014) and Neogene grains eroded from leucogranites (e.g. Hodges, 2000 and

159   references therein). Within the Indian plate, grains 1500-2300 Ma are characteristic of the Lesser

160   Himalaya, and 300-1250 Ma characteristic of the Greater and Tethyan Himalaya, although not uniquely

161   so (Clift et al., 2019). By contrast, zircons from the KLIA are exclusively aged 40-200 Ma, whilst the

162 southern Asian margin (the Karakoram and to the east the Lhasa Block) also have a high proportion of

163 grains of such age, but also with some Neogene grains, and older grains stretching to the Precambrian,

164 derived from the substrate into which the Mesozoic-Paleogene plutons intruded (e.g. Zhuang et al.,

165 2018 and references therein).

166 The old continental crust of the Indian plate has a mean ε_{Nd} value of -15 for the Greater Himalaya, -22

167 for the Lesser Himalaya, and -11 for the Tethyan Himalaya (Ahmad et al., 2000; Deniel et al., 1987;

168 Richards et al., 2005; Robinson et al., 2001; Zhang et al., 2004). By contrast, the Asian and intra-oceanic

169 arc terranes have more positive values, reflecting the dominance of Mesozoic-Paleogene plutons: the

170 KLIA has values around +5 (Bignold and Treloar, 2003; Khan et al., 1997; Khan et al., 2004; Khan et al.,

171 2009), whilst the Karakoram, which consists of both old sedimentary and metamorphic rocks as well as

172 younger plutons, has an average value around -9.6 (Mahéo et al., 2009; Miller et al., 1999). Data from

173 the Lhasa Block are mainly from the central and eastern part of the orogen: the Gangdese /

174 Transhimalaya have values ranging from +0.9 to 5.5 for the Mesozoic granitoids and +2.4-8.5 for the

175 Paleocene-Eocene granitoids in contrast to the Oligocene-Miocene granitoids with values of -9.4 to 5.5

176 (Ji et al., 2009; Pan et al., 2014), whilst the continental substrate into which these plutons intruded have

177 an average recorded ε_{Nd} value of -9 (Pan et al., 2014; Zhu et al., 2009; Zhu et al., 2012).

178 *2.1.2. Tectonic evolution.*

179 Prior to India-Asia collision, India was subducting beneath Asia as Neo-Tethys closed, with the KLIA

180 located between the two continents in the west. The timing of India-Asia collision, and whether the

181 island arc collided with India or Asia first, is disputed; a majority of researchers consider India-Asia

182 collision occurred around 55-60 Ma (see review in Hu et al., 2016 and references therein) with other

183 estimates extending to c. 35 Ma or 25-20 Ma (Aitchison et al., 2007; Bouilhol et al., 2013; van

184 Hinsbergen et al., 2012).

185   The west differs from the better studied east and central part of the orogen in both the presence of the

186   KLIA, and in the timing of exhumation of the Indian plate. In the west, a tectonic wedge consisting of the

187   KLIA, ophiolitic melange and thrust slices of Lesser Himalayan and Tethyan correlatives of the Indian

188   plate was in position and thrust over the Indian plate foreland prior to 47 Ma. Thereafter, Indian plate

189   Lesser-, Greater- and Tethyan Himalayan correlatives were exhumed from beneath the wedge (DiPietro

190   et al., 2008), predominantly during the Paleogene with a pulse of deformation also in the earliest

191   Miocene, ~20 Ma (Argles et al., 2003, and references therein; DiPietro et al., 2021). Substantial rapid

192   exhumation of the Indian plate hinterland is not recorded after this time, except in the Nanga Parbat

193   region (Fig 1C), a syntaxis of Lesser, Greater and Tethyan Himalayan lithological correlatives, where

194   rapidly accelerating exhumation is recorded over the Pliocene (e.g., Schneider et al., 2001). Thrusting

195   and exhumation propagated south towards the foreland in the mid or late Miocene, continuing into the

196   Pliocene (Burbank and Tahirkheli, 1985; Yeats and Hussain, 1987).

197   To the north of the Indian plate, moderate exhumation is recorded from Eocene times in the Kohistan

198   Island arc (Van Der Beek et al., 2009) and by contrast, the Karakoram of the Asian plate records periods

199   of rapid exhumation around 27-35 Ma, 13-17 Ma, 7-8 Ma and 3.3-7.4 Ma (Dunlap et al., 1998; Wallis et

200   al., 2016; Zhuang et al., 2018).

201   *2.2. Foreland basin geology*

202   In Pakistan, current basinal environments along which the modern Indus River flows, consist of (1) the

203   peripheral foreland basin that strikes east-west along the southern margin of the orogen, and (2) the

204   north-south striking Lower Indus axial foreland basin along which the Lower Indus River debouches into

205   its delta in the Arabian Sea (Fig. 1A).

206   *2.2.1 Peripheral foreland basin*

207 Foreland basin stratigraphy is for the most part invariant along strike in the orogen, with local minor

208 facies variation, although formation names differ. In Pakistan, the Paleogene has a number of formation

209 names for equivalent units, in different areas (Pivnik and Wells, 1996). We adopt the formation names in

210 our area of study, which for our Paleogene samples is the Hazara-Kashmir syntaxis (HKS) (Figs. 1A and

211 B), with the stratigraphy as recorded in Table 1. At this location, the Paleocene Lockhart Limestone is

212 overlain successively by the latest Paleocene (57-55 Ma) Patala Formation, the early Eocene (55-53 Ma)

213 Margala Hill and Chorgali Formations, and the early-Mid Eocene (53-43 Ma) Kuldana Formation (Baig

214 and Munir, 2007; Bossart and Ottiger, 1989; Ding et al., 2016b; Qasim et al., 2018). These formations,

215 which stretch from marine facies to the transitional Kuldana Formation, are separated from the

216 overlying continental alluvial facies by a late Eocene-Oligocene unconformity. Above the unconformity,

217 there is the Murree Formation, also called the Balakot Formation in the HKS. In this syntaxis, the Murree

218 Formation has a latest Oligocene maximum depositional age (MDA) as determined by the two youngest

219 zircons within error, with a weighted mean U-Pb age of 22.6 ± 1.0 Ma (this study, section 4.2) from a

220 sample collected near Paras, north of Balakot (Fig. 1B), supported by a grain dated at 22.7 +/- 0.4 Ma

221 (Ding et al 2016b) from a section 15 kms south at Muzaffarabad (Fig. 1B). South-west of the Hazara-

222 Kashmir syntaxis, at Murree hill station (MHS) (Fig. 1B), detrital mica Ar-Ar ages indicate an MDA of <24

223 Ma (this study, section 4.3). These MDAs are in agreement with the early Miocene dating of the Murree

224 Formation to the south, based on mammal fossils (Shah, 2009). Further south, in the Kohat and Potwar

225 Plateaus (Fig. 1A) are the alluvial Kamlial Formation and overlying Siwalik Group, subdivided into the

226 Chinji, Nagri and Dhok Pathan Formations (see Table 1 for stratigraphy). These formations are dated by

227 magnetostratigraphy (Johnson et al., 1985), at 18-14 Ma, 14-11 Ma, 11-8.5 Ma, and <8.5 Ma,

228 respectively.

229 *2.2.2 Lower Indus axial Basin*

230 The stratigraphy of the Lower Indus Basin in the Sulaiman and Kirthar regions are broadly correlative

231 (Shah, 2009). It encompasses the early Eocene Ghazij Formation, the middle-late Eocene Kirthar Group,

232 the Oligocene-early Miocene Chitarwata Formation, the late Early to middle Miocene Vihowa

233 Formation, and the middle Miocene-Pliocene rocks of the Siwalik Group (Roddaz et al., 2011; Shah,

234 2009; Zhuang et al., 2015), as denoted in Table 1. Facies are predominantly marine until the Chitarwata

235 Formation which transitions up from deltaic to fluvial facies. Fluvial facies then persist until the top of

236 the section.

237 **2.3 Paleodrainage models**

238 *2.3.1 The early drainage configuration of the palaeo-Indus: evidence from the Indus Fan sedimentary*

239 *archive*

240 The oldest eastern Indus Fan sample (IODP 355, U1456 and 1457, Fig 1A) to have been subject to

241 detrital zircon U-Pb analyses is 15 Ma. This shows evidence of input from the Karakoram (Zhou et al.,

242 2022), indicating the drainage basin of the palaeo-Indus stretched as far back as the Shyok Suture Zone

243 by this time (Fig 1C). The oldest sample subjected to detrital zircon U-Pb dating in the western part of

244 the Indus Fan (ODP 731, Fig 1A) is ~ 30 Ma. This sample shows evidence of input from the KLIA/Asian

245 plate (undifferentiated), indicating that the river stretched back at least beyond the Indus Suture Zone

246 (Fig 1C) by that time (Feng et al., 2021). Likewise, Mid Eocene Owen Ridge sediments from DSDP 224

247 (Fig 1A), considered to be early Indus Fan deposits (Clift et al., 2001a; Clift et al., 2002a), show bulk rock

248 ε_{Nd} signatures and K-feldspars with Pb isotope compositions indicative of derivation from north of the

249 Indian plate (Clift et al., 2001a). This indicates that the river's drainage basin stretched back as least as

250 far as the Indus Suture Zone and KLIA at this time.

251 *2.3.2. The early drainage configuration of the upper axial palaeo-Indus: evidence from the Indus Suture*

252 *Zone molasse.*

253   Clift et al. (2001b) considered that various isotopic provenance datasets and palaeocurrents in Indus

254   suture zone sedimentary rocks of early Eocene age indicated contribution from the Lhasa Block to the

255   east, requiring along strike east to west flow along the suture zone at that time. However, Najman

256   (2006) argued that an alternative source with a suitable signature could potentially be that of the

257   Karakoram, located north of the suture zone sediments under discussion, and therefore not requiring

258   along-strike transport and axial flow. Sinclair and Jaffey (2001) considered their facies analyses of the

259   suture zone sediments indicated internal rather than through-flowing drainage until at least the early

260   Miocene. Later, Henderson et al. (2010) reported that white micas, interpreted as Indian-plate derived,

261   first occurred in the same suture sedimentary rocks as Asian-derived zircons, in suture zone sedimentary

262   rocks dated <23 Ma. From these mixed source sedimentary rocks, and accompanying facies analysis,

263   they considered the Indus River was flowing in the suture zone at that time. However, it should be noted

264   that (1) micas were also recorded in older suture zone sedimentary rocks but they were of too small

265   grain size to analyse, (2) Indian plate material with low muscovite fertility such as from the Tethyan

266   Himalaya may well have contributed to the suture zone rocks earlier and (3) an open question remains

267   as to why the first appearance of micas interpreted as Indian-derived, was not also accompanied by an

268   influx of Paleozoic and older zircons, also typical of the Indian plate. Whilst subsequently, such old

269   zircons, interpreted as Indian rather than Asian-derived, have been documented in suture zone

270   sediments as old as ca. 50 Ma (Bhattacharya et al., 2020), nevertheless they are not present in the

271   samples analysed for white mica Ar-Ar analyses by Henderson et al (2010). Whilst mineral sorting due to

272   different hydraulic regimes of zircon versus mica (Malusà et al., 2016) might explain the difference, we

273   suggest that, with the benefit of subsequent better characterisation of the ages of micas from the

274   southern margin of the Asian plate (Zhuang et al 2018), an Asian Karakoram provenance might provide

275   an alternative provenance for these micas. Regardless, mixed Indian-Asian provenance, unaccompanied

276   by facies data indicating deposition in a major river, does not indicate east-west through-flow of

277   drainage. Bhattacharya et al. (2020) demonstrated from provenance data that detritus from the east

278   was transported west by ca 27 Ma. Thus we may conclude that an axial upper Indus flowed west by

279   Oligocene times. Prior to that the suture zone was a depocentre, but it may have been externally or

280   internally drained.

281   *2.3.3. Early drainage configuration of the upper transverse palaeo-Indus River: evidence from the*

282   *peripheral foreland basin deposits*

283   In the peripheral foreland basin, detrital blue-green hornblende considered to be derived from the KLIA,

284   is first recorded in the Kohat and Potwar plateaus from 11 Ma (Nagri Formation), interpreted as palaeo-

285   Indus deposits (Abbasi and Friend, 1989; Cerveny and Johnson, 1989). Ullah et al. (2015) applied

286   geochemistry and petrography to the Chinji Formation (14-11 Ma) to record material from the KLIA and

287   Indus suture zone. Based on petrography, Najman et al. (2003) recorded arc-derived detritus in the

288   Potwar plateau from the start of their studied section at 18 Ma, from which they interpreted that this

289   time represented the first arrival of sediment from the Upper Indus River to the foreland basin in this

290   region. Still later work (Ding et al., 2016b; Qasim et al., 2018) recorded arc-derived zircons in the

291   foreland basin latest Paleocene to Early Eocene Margala Hill and uppermost Patala Formations,

292   indicating derivation from north of the Indus Suture Zone / Main Mantle Thrust since at least 55 Ma.

293   Whilst the above provenance data indicates derivation from material as far north as the KLIA since

294   Eocene times, whether these rocks represent the deposits of the palaeo-Indus is debated (Cerveny et

295   al., 1989; Willis, 1993; Zaleha, 1997). Chirouze et al (2015) proposed a Lhasa Block origin for detrital

296   zircons with old fission track ages in the Chinji Formation. This would indicate that the contributing

297   drainage basin stretched into the Shyok Suture Zone and Asian plate by this time, and was therefore

298   likely the palaeo-Indus. However, we suggest that such grains may also be derived from the Indian

299   Himalayan units south of the KLIA, as arguable by their occurrence in the Siwalik foreland basin

300   sedimentary rocks of Nepal, that were deposited by rivers which did not stretch back to Asia (Bernet et

301   al., 2006).

302   However, more definitive evidence of deposition from the palaeo-Indus comes from detrital mica Ar-Ar

303   data. Lag times of detrital mica Ar-Ar ages from Kamlial Formation Potwar Plateau sedimentary rocks

304   indicate rapid exhumation of the upland source region from 16-14 Ma (Najman et al., 2003). The

305   exhuming source area was interpreted by those authors to be the Karakoram and/or Nanga Parbat

306   region, consistent with both bedrock data from those regions (Treloar et al., 2000; Zhuang et al., 2018

307   and references therein). Due to their locations, derivation of micas from either location strongly

308   suggests transport by a palaeo-Indus. Furthermore, detritus delivered by possible ancient smaller

309   tributaries draining only the Indian plate and arc would have had a distinct and different signature, with

310   a higher proportion of Indian plate detritus, for example the Mid Miocene Kamlial Formation sample

311   CP96-6A from Najman et al. (2003), and presumably those samples from the Eocene Kuldana Formation

312   with a high proportion of old zircons at Muzaffarabad (Ding et al., 2016b) (see section 5.2 for further

313   discussion).

314   *2.3.4. Evolution of the Lower Indus palaeodrainage*

315   Within the basin, the position of the Ganges-Indus drainage divide over time is long debated, with

316   various authors proposing that parts of the current Gangetic catchment used to flow into the Indus Fan

317   (e.g. DeCelles et al., 1998), and the current Indus River catchment into the Bengal Fan (e.g. Burbank et

318   al., 1996) at various times. Clift and Blusztajn (2005) noted a change to more negative ε_{Nd} values in the

319   Indus Fan at 5 Ma, which they interpreted as the drainage diversion of the major Indian-plate draining

320   Punjabi Indus River tributary system of the Jhelum, Chenab, Ravi and Sutlej rivers (Figs. 1A and C) from a

321   previous routing towards the Ganges and the Bengal Fan to the east.

322   However, the above argument was countered by Chirouze et al. (2015) who looked at both spatial and

323   temporal trends at the range front and Indus Fan. They considered that the change in the signal was due

324   to differential exhumation in the hinterland rather than drainage re-organization. They compared ε_{Nd}

325   data between the range front and Indus Fan for both the present day and the Miocene (using Chinji

326   Formation foreland basin data for the Miocene range front). They recorded a spatial variation of four ε_{Nd}

327   units between the range front and the Indus Fan for both mid-late Miocene times and modern day

328   (Miocene range front and Indus Fan values at -6 and -10 respectively; modern day range front and Indus

329   Fan values at -10 and -14 respectively. This suggests a stable drainage pattern for the lower Indus since

330   at least the mid-late Miocene. From the above data they noted a negative shift of ~3 ε_{Nd} units between

331   Miocene and the modern day at both the range front (comparison of Miocene foreland basin

332   sedimentary rocks with modern day Upper Indus values) and a similar shift in the Indus Fan. From this

333   temporal shift they therefore concluded that the variation over time was due to the changing

334   exhumation rates of the contributing source regions, with the exhumation and thus contribution of the

335   Karakoram / Indian plate syntaxial Himalaya increasing at the expense of the more positive KLIA (Table

336   1) to explain the shift in ε_{Nd} values in the Indus Fan at 5 Ma. They supported their proposal of variations

337   in exhumation using detrital zircon fission track (ZFT) data, interpreting a decrease in older ZFT ages

338   after 12 Ma as due to decreased input from the KLIA. Later, the original proponents of the drainage

339   capture hypothesis (Clift and Blusztajn, 2005) concurred with the view of Chirouze et al. (2015) that

340   changes in the tectonics of the hinterland was the more likely cause of the geochemical change in the

341   Indus Fan at 6 Ma (Clift et al., 2019; Zhou et al., 2022) thus the time when the Punjab tributary system

342   joined the trunk Indus remains unknown. It is towards this question, namely the evolution of the

343   downstream Indus, that this paper focusses.

344   The location of the exit of the Indus River to the ocean in the past retains a level of uncertainty. Today

345   the Indus River debouches to the Arabian sea at the south of the Lower Indus axial Basin. These deposits

346   are recorded in eastern Sulaiman and Kirthar regions of the Lower Indus Axial Basin (Welcomme et al.,

347   2001) (Fig 1A). Zhuang et al. (2015) show that zircons from the KLIA are recorded in these sediments

348   from at least early Oligocene times; they considered that detrital zircon U-Pb data indicate input from

349   the Karakoram from at least Mid Miocene times, and that Sr-Nd data indicate a palaeo-Indus origin from

350   50 Ma. Roddaz et al. (2011) carried out mixture modelling on their Sr-Nd data and concluded that there

351   was an appreciable input from the Karakoram since 50 Ma.

352   However, Palaeogene deltaic facies have also been identified in the Katawaz remnant ocean Basin (Fig

353   1A) to the west (Qayyum et al., 2001). In view of the differing compositions and provenance between

354   these two deltaic systems, Roddaz et al. (2011) proposed two river-delta-fan systems, with the Katawaz

355   system debouching into the Khojak submarine fan and the sediments of the Lower Indus Axial Basin

356   debouching into the Indus Fan. Provenance data from the Katawaz rocks show that that drainage basin

357   stretched back at least as far as the KLIA by Miocene times (Carter et al, 2010) with a paucity of data

358   currently precluding earlier documentation. For a full evaluation of the Indus river-delta-fan system and

359   the spatial evolution, more data are needed from the Katawaz basin; data presented in this paper

360   provide a direct comparison between peripheral foreland basin records and terminal sinks in the delta

361   and ocean.

362

363   **3. Methods**

364   *3.1 Rationale and approach*

365   To determine when the Punjab tributary system joined the trunk Indus, we leverage that fact that the

366   tributaries have a very different drainage basin lithology to the trunk Indus; the former includes only

367   Himalayan units, whilst the drainage basin of the latter includes also the KLIA and Asian plate (Fig. 1C),

368   which have very different isotopic and geochemical signatures to the Indian plate (Table 1). This

369   difference is clearly reflected in both the Sm-Nd and zircon U-Pb characteristics of the trunk Indus river

370   versus the Punjabi tributary system: Figs 2and 3A (inset) shows that, compared to the modern Indus

371   trunk river, the Punjabi tributaries have a more negative εNd value and a much lower proportion of

372   young arc-aged grains (Alizai et al. 2011, Chirouze et al 2015), a signature which extended back into the

373   ancient sedimentary record (Exnicios et al., 2022; Najman et al., 2009).

374   We took a similar approach to Chirouze et al (2015) in hypothesising that prior to the time when the

375   Punjab tributary system joined the trunk Indus River, the sedimentary repositories upstream and

376   downstream of the confluence should look similar in terms of provenance. After the time when the

377   tributary system joined the Indus River, the repository upstream of the confluence should remain similar

378   (unless synchronously affected by a tectonic-induced change in the hinterland), but the downstream

379   repository should show increased input from Himalayan Indian plate units.

380   We therefore made comparison between data upstream (our new foreland basin data) and published

381   data downstream of the Punjab tributary system. Previous work used the Indus Fan as the downstream

382   comparative repository. We use both the deltaic record in the Sulaiman and Kirthar region, and the

383   Indus Fan archive, since onshore sedimentary archives are typically more prone to diagenetic alteration

384   compared to marine records, whilst distal deposits are more prone to the effects of hydraulic sorting

385   (e.g., Garzanti et al., 2020) and contain evidence of subordinate extraneous (non-Indus River) sources to

386   the Himalayan orogen, such as the Deccan Traps of peninsular India input to the Indus Fan (Clift et al.,

387   2019; Garzanti et al., 2020; Yu et al., 2019). The Indus Fan record is a composite repository of material

388   recovered from the Owen Ridge and Western Fan from DSDP 224 (Eocene-Miocene) and ODP 720, 722

389   and 731 (Eocene-Pleistocene) sites, and IODP 355 sites of U1456 and1457 of the Eastern Fan (Neogene

390   only) (Clift et al., 2019; Feng et al., 2021; Zhou et al., 2022) (Fig. 1A).

391   Our dataset builds on the previous work of Chirouze et al. (2015) in two ways. Firstly, it expands the

392   time range from the previous mid Miocene study of the Pakistan peripheral foreland basin to now

393   include foreland basin rocks from Eocene to late Miocene. This allows a more complete assessment of

394   the evolution of the lower Indus to be determined. Secondly, we incorporate not only ε_{Nd} data from

395   mudstones, but also new and previously published zircon U-Pb data to assess provenance, and mica

396   $^{40}Ar/^{39}Ar$ data to assess exhumation. Therefore, in addition to using both onshore and offshore

397   repositories to limit the potential effects of fertility, diagenetic, and hydraulic sorting biases, our multi-

398   proxy approach provides additional mitigation since: 1) zircons are resistant to diagenesis; 2) we assess

399   evidence from both the mud and sand grain size fractions with the use of both bulk and single grain

400   approaches and 3) we obtain data from both zircon and mica grains which respond differently to the

401   hydraulic regime (e.g., Garzanti and Andò, 2019; Garzanti et al., 2009; Malusà et al., 2016). Furthermore,

402   since white mica is rare in the KLIA, exhumation patterns of the Karakoram and Indian plate Himalaya

403   can be considered in isolation using this technique, unbiased by potential issues surrounding dilution

404   and fertility.

405

406   ***3.2. Samples and analyses***

407   *3.2.1 Samples*

408   We analysed 5 sandstones for detrital zircon, 10 mudstones for Sr-Nd isotopes, and 3 sandstones for

409   mica $^{40}Ar/^{39}Ar$. The locations of analysed samples (Figs. 1A and B) are from the Kuldana Formation in the

410   HKS at Paras north of Balakot, the Murree Formation in both the HKS and at Murree Hill Station (MHS),

411   and the Kamlial, Chinji and Nagri Formations from the Chinji section on the Potwar Plateau, the latter

412   being the same location from which Chirouze et al (2015) took their samples. A summary of our sample

413   information is tabulated in S1. Our samples from the Kuldana Formation are structurally imbricated

414   within the Murree Formation (Najman et al., 2002). Originally, Najman et al (2002) considered these

415 structural imbrications to be Patala Formation, based on the work of Bossart and Ottiger (1989) who did

416 not recognise the Kuldana Formation. However, more recent detailed mapping (Ding et al., 2016b) and

417 the better agreement of biostratigraphic ages from the structural imbricates (early-mid Eocene; Bossart

418 and Ottiger (1989)) with the Kuldana Formation rather than Patala Formation (section 2.2.1), suggests

419 reassignment of these imbricates from the Patala to the Kuldana Formation.

420 *3.2.2 Sr-Nd bulk analyses*

421 Sr and Nd isotope analyses on bulk mudstones were carried out at the NERC Isotope Geosciences

422 Laboratory, Keyworth, Nottingham. Samples were leached in dilute acetic acid in order to remove

423 carbonate material, then dissolved using HF-HNO3 and converted to chloride form. Sr and a bulk REE

424 fraction were separated using AG50x8 cation columns, and Nd was separated from the bulk REE using

425 LN-SPEC columns. Sr and Nd were analysed on a Thermo Scientific Triton mass spectrometer.

426 *3.2.3 Zircon U-Pb analyses*

427 Detrital zircon U-Pb ages were acquired using laser ablation ICPMS, at the London Geochronology

428 Centre, University College London. To avoid bias, polished grain mounts were made, without hand

429 picking, directly from Diidomethane sink fractions with a grain size ≤ 300 µm. Each laser spot (25 µm)

430 was placed on the outermost parts of each grain to target the youngest growth stage. Between 150-320

431 grains were analysed for each sample, providing statistical confidence of detecting all component ages.

432 Data were processed using GLITTER v4.4 data reduction software using age standard bracketing to

433 correct for mass fractionation. Between 8 and 15% of ages were rejected, due to high discordance from

434 lead loss, zoning or mixing of growth zones. One exception was the Chinji Formation that contained an

435 unusually high number (60%) of discordant grains. Most of these discordant grains are associated with

436 ages between 75-120 Ma and consistent with lead loss, likely due to source weathering.

3.2.4 Muscovite Ar-Ar analyses

438   Muscovite Ar-Ar ages were analysed at the Argon Geochronology Laboratory at VU University

439   Amsterdam, Netherlands. Individual grains ranging from 125-1000 μm were handpicked under a

440   binocular microscope to avoid obvious weathering or inclusions. After irradiation at the Oregon State

441   University TRIGA nuclear reactor, total fusion analyses were carried out with a ThermoFisher Scientific

442   Helix MC plus multi-collector mass spectrometer, fitted with 10^{13} Ohm amplifiers. Data reduction was

443   done using ArArCALC2.5 (Koppers, 2002).

444   Detailed methodologies are provided in SI 1, and results are reported in Tables S1 (Sr-Nd data), S2

445   (zircon U-Pb data) and S3 (mica Ar-Ar data).

446

447   **4.   Results and integration with published data**

448   ***4.1 Sr/Nd bulk (Figs. 2 and SI Fig S1, Table S1)***

449   There is little significant variation in ε_{Nd} values from the Eocene Kuldana Formation through to the late

450   Miocene Nagri Formation, with values ranging between -7.0 to -9.2 (Fig. 2A). The exception to this

451   overall similarity is the Murree Formation at MHS, with a value of -13.8. We note that previous work for

452   the Chinji Formation records values of -3.8 to -7.7 (Chirouze et al., 2015); this difference could perhaps

453   reflect the previous use of sand compared to analysis of muds in the current research (see Jonell et al.,

454   2018 for further discussion). There are no modern-day data available for the range front. The Upper

455   Indus has a value of -10.8 at Besham (Clift et al., 2002b) located just downstream of the Kohistan arc

456   (Fig. 1B and C) and we can extrapolate that values should be more negative than this at the range front,

457   after the river has passed over the Greater and Lesser Himalaya. Values at the delta front at Thatta are -

458   14.9 (Clift et al., 2002b).

459   We carried out mixture modelling on the foreland basin material (SI Fig. S1). The mixture modelling is

460   complicated by the number of end member contributors; today sediment in the Upper Indus River

461   contains material from the Lhasa Block, Karakoram, KLIA, suture zone, and the Indian plate units of the

462   Greater-, Lesser- and Tethyan Himalayan correlatives. Overlapping signatures of some units (e.g.

463   between the Karakoram and Tethyan Himalaya, and between the KLIA and ophiolitic melange of the

464   suture zone) also adds uncertainty. We started with the premise that, from the zircon data we are

465   confident that the foreland basin contains material from the KLIA (section 4.2.) from the oldest

466   sediments studied, namely the early-Mid Eocene Kuldana Formation. That therefore forms the apex of

467   our model, and various mixture couplings are calculated with this apex and other potential end

468   members. The modelling shows that all data can be explained by a mix of Indian plate and KLIA inputs,

469   and contribution from the Karakoram and Lhasa Block is equivocal. The Murree Formation sample from

470   MHS requires considerable input from Greater Himalayan lithological correlatives.

471   The Sr-Nd compositions of the samples plot on trends that are consistent with simple mixing between

472   mafic and more evolved sources. There is some scatter in the data towards high Sr^{87}/Sr^{86} values that

473   may result from weathering or diagenesis. However, we are confident that the dominant trends reflect

474   changes in provenance, as described above.

475   ***4. 2 Detrital zircon U-Pb analyses (Fig 3, SI Figs S2 and S3, Table S2)***

476   We compile our new data from the Murree Formation at Paras north of Balakot in the HKS and at MHS

477   (< 24 Ma), and from the Kamlial (18-14 Ma), Chinji (14-11 Ma) and Nagri (11-8.5 Ma) Formations in the

478   Potwar Plateau, with previously published data from the Kuldana and Murree Formation rocks at

479   Balakot, Muzaffarabad and Kotli in the HKS and at MHS (Awais et al., 2021; Ding et al., 2016a; Qasim et

480   al., 2018) and modern river data collected at the MCT-correlative (Khairabad Thrust) at the range front

481   at Attock (Alizai et al 2011, Clift et al 2022) (Fig. 1B). We keep our observations of comparisons broad

482   and conservative in nature, since different approaches to both mineral separation and data processing

483   procedures by different labs can cause variation in proportions of different populations. We begin our

484   summary at the marine to continental transition (the Kuldana Formation, section 2.2.1). We focus on

485   the 40-200 Ma "arc-aged" population characteristic of the KLIA and Karakoram, and the older grains

486   typical of the Indian plate and Karakoram, with emphasis on the 1500-2300 Ma population typical of the

487   Lesser Himalayan lithological correlatives and 300-1250 Ma population typical of the Greater Himalayan

488   lithological correlatives (section 2.1.1, Table 1).

489   With the exception of the Murree Formation (which we portray separately in Fig 3B and discuss

490   separately in section 5.2), the proportions of the 40-200 Ma "arc-aged" populations remain approaching

491   or above 50% throughout the Neogene to present day. There is much variation within the Eocene

492   Kuldana Formation, with nevertheless a number of samples also showing a majority of grains to be arc

493   aged (Fig. 3A, Table 1). By contrast, the Murree Formation has a very low proportion of grains in the 40-

494   200 Ma range in all samples analysed from MHS, Muzaffarabad and Balakot, although not at Paras north

495   of Balakot in the HKS (Fig 1B, Fig 3B and SI Fig S2). Instead, these Murree Formation samples from MHS,

496   Muazaffarabad and Balakot have a high proportion of grains with ages typical of the Greater Himalaya.

497   In contrast to the modern-day river sample at Attock (Fig. 3C, Fig 1B), there is no 1500-2300 Ma

498   population typical of the Lesser Himalayan lithological correlatives, in any of the formations.

499   *4.3 Mica Ar-Ar (Fig 4, SI Fig. S4, Table S3)*

500   We have integrated our new data from the Murree Formation at MHS, Chinji and Nagri Formations with

501   previous data from the Murree Formation in the HKS at Paras north of Balakot (Najman et al., 2001) and

502   Kamlial Formation (Najman et al., 2003) (SI Fig. SI4). We note the following, bearing in mind that the

503   number of grains analysed for the Murree Formation at Paras north of Balakot (n=257) and the Kamlial

504   Formation (n=277) are considerably higher than for the Murree Formation at MHS, Chinji and Nagri

505 samples (n=59, 94 and 43 respectively), resulting in more confidence that the Balakot and Kamlial

506 Formation datasets more completely capture the complete spectrum of ages:

507 The youngest grain in the Murree Formation at Paras in the HKS is 24.6 +/- 0.7 Ma, the weighted mean

508 of the youngest two grains overlapping within error at two sigmas is 24.8 Ma +/- 1.4 Ma and the

509 youngest peak population is 37 Ma. Pre-Cenozoic ages extend to >1500 Ma. Further south, the youngest

510 grain in the Murree Formation at MHS is 23.7 +/- 0.1 Ma, which also forms one of the two youngest

511 grains overlapping within error at 2 sigmas (weighted mean 23.85 +/- 0.12 Ma. The youngest peak

512 population is 24-28 Ma. Pre-Cenozoic ages extend to ca 450 Ma. The youngest grain for the Kamlial

513 Formation is 14.5 +/- 0.7 Ma, and weighted mean of the youngest two grains within error at 2 sigmas is

514 15.00 +/- 1.10a. The youngest peak population is 18 Ma and Pre-Cenozoic ages extend to ca 450 Ma. The

515 lowest Chinji Formation sample (CP96-7A, Najman et al 2003, dated at 13.9 Ma) has a youngest grain at

516 14.1 +/- 0.7 Ma and this also forms one of the two youngest grains within error at 2 sigmas (weighted

517 mean 14.43 +/- 0.81 Ma). Pre-Cenozoic grains extend to 400 Ma. Our new sample from the Chinji

518 Formation has a youngest grain of 16.74 +/- 0.1 Ma, the weighted mean of the two youngest grains

519 overlapping within error at 2 sigmas is 25.95 +/0 0.10 Ma, the youngest peak population is 28-29 Ma,

520 and Pre-Cenozoic ages extend to ca 450 Ma. The youngest grain in the Nagri Formation is 17.9 +/- 0.14

521 Ma, the weighted mean of the two youngest two grains overlapping within error at 2 sigmas is 19.69 +/-

522 0.12 Mathe youngest peak population is 21 Ma and Pre-Cenozoic ages extend to ca 200 Ma.

523 Rapid exhumation determined from short lag times was determined for the Kamlial and lowest Chinji

524 Formation, between 16-14 Ma (Najman et al, 2003) (Fig. 4). Lack of independent depositional age

525 constraints precludes calculation of lag times for the newly analysed Murree, Chinji and Nagri Formation

526 samples. Up section from the Kamlial Formation, there is no evidence of grain ages approaching

527   depositional age, until the modern river sample at Thatta, although the number of grains analysed is

528   relatively small.

529

530   **5.   Interpretations of the evolution of the Lower Indus drainage**

531   *5.1. When did the Punjabi tributary system join the paleo-Indus trunk river?*

532   As outlined in our rationale and approach (section 3.1), we determine when the Punjab tributary system

533   joined the main trunk river, by a comparison of provenance data from upstream and downstream of the

534   present day confluence, leveraging the fact that unlike the palaeo-Indus trunk River, the tributaries

535   drain only the Indian plate terranes (Fig 1C), and thus have a different provenance signature (section

536   3.1, Figs 2 and 3A inset).

537   As schematically presented in Fig 5, the following evidence should be met, at the time the tributary

538   system joined the trunk Indus:

539   (1) Prior to the time that the Punjab tributary system joined the Indus catchment, the proportion

540   of Indian plate detritus delivered to the Indus River should be comparable at the range front and

541   at the river mouth, i.e. upstream and downstream of where the Punjab tributary system now

542   joins the modern Indus.

543   (2) After the time when the Punjab tributary system joined the Indus River, the proportion of Indian

544   plate material in the Indus River downstream of the confluence with the Punjab Rivers should a)

545   increase relative to the downstream's previous pre-reorganisation proportion and b) be greater

546   than coeval sediments upstream. However, the proportion of Indian plate material in the

547   upstream should remain constant, pre and post the proposed drainage reorganisation.

548   For the above predictions to be explored, Indian plate, versus Karakoram, versus KLIA must be

549   differentiable in the foreland basin detritus. Table 1 provides the typical zircon U-Pb and ε_{Nd} signatures

550   of these units, alongside a summary of equivalent data from the peripheral foreland basin, and

551   downstream in both the Sulaiman-Kirthar region and Indus Fan. Figs 2 and 3A inset show the difference

552   between the modern trunk Indus which drains the Asian plate, arc and Indian plate, versus the modern

553   Punjabi tributary system which drains, for the most part, only the Indian plate.

554   For the interpretations made from this upstream-downstream comparison to be valid, the rocks at the

555   evaluated locations must be the products of the palaeo-Indus. Whilst all three repositories studied, the

556   peripheral foreland basin, the Lower Indus Axial Basin, and the Indus Fan, show evidence of derivation

557   from at least as far north as the KLIA since Eocene times, we acknowledge evidence for input from north

558   of the Shyok suture zone can be equivocal (see sections 2.3.1, 2.3.3 and 2.3.4).

559   Below, we summarise the salient points regarding the upstream and downstream repositories that are

560   relevant to the characteristics required to document the timing of conjoinment of the Punjabi tributary

561   system with the trunk Indus River as described above. We discuss the Murree Formation which is

562   anomalous at MHS, Muzzafarabad and Balakot, but not at Paras, separately in section 5.2.

563   *5.1.1. Comparison of the upstream peripheral foreland basin material with the downstream repositories*

564   *in terms of Sr-Nd data*

565   Our data from the upstream (peripheral foreland basin) show that values have remained broadly

566   constant from the start of our studied record in the early-Mid Eocene Kuldana Formation (Fig. 2A), until

567   the late Miocene Nagri Formation, when values become a little more negative. εNd(0) values in the

568   downstream repositories are similar to the upstream in the early Eocene. However, values in the

569   downstream repositories become more negative compared to the upstream, by Mid Eocene in the Indus

570   Fan and around the Eocene-Oligocene boundary in the Lower Indus Axial Basin (Fig. 2B). This shift

571   indicates a greater input of material from the Indian plate Himalayan terrane at this time.

572   From the more negative $\varepsilon Nd(0)$ values recorded below compared to above the confluence throughout

573   the Neogene, we interpret that the Punjabi tributary system has drained into the palaeo-Indus

574   throughout the Neogene, and that the present drainage configuration was therefore established during

575   the Paleogene.

576   The consistency of εNd values from the Eocene to the Neogene in the upstream repository, in contrast

577   to the shift to more negative values in the downstream repositories should reflect the time when the

578   Punjabi tributary system joined the trunk Indus River. However, the difference in the time of the

579   downstream shift, at the Eocene-Oligocene time in the Lower Indus axial basin delta deposits and in the

580   mid Eocene in the Indus Fan indicates that more research is required before we can pinpoint the exact

581   time that the tributary system joined the trunk Indus. Nevertheless, with available data we can conclude

582   that the tributaries joined in the trunk Indus at or before the start of the Oligocene (Fig 5).

583   *5.1.2. Comparison of the upstream peripheral foreland basin material with the downstream repositories*

584   *in terms of detrital zircon U-Pb data*

585   Although intraformational variability, lack of data from the Oligocene in the peripheral foreland basin,

586   and lack of data from the Eocene in the downstream repositories limits the comparison, the data are

587   consistent with the interpretations determined the Sm-Nd data, that the Punjabi tributary system joined

588   the trunk River Indus by Oligocene times (section 5.1.1, Fig 5): The proportion of 40-200 Ma arc-aged

589   grains remains high throughout the Miocene in the peripheral foreland basin, and these values are

590   higher compared to Oligocene-Pliocene values in both downstream repositories (Fig. 3A and C, Table 1).

591   Data from the Eocene peripheral foreland basin is highly variable. However, at least some samples have

592   a proportion of arc-aged grains similar to the proportions of the Neogene peripheral foreland basin,

593   consistent with the pattern shown in the Sm-Nd data.

594   SI Figure SI 3 illustrates the river's evolution well, particularly by comparison to the Lower Indus Axial

595   Basin. Downstream samples have a greater affinity to Indian plate rocks and the modern Indus at its

596   mouth at Thatta, compared to the upstream peripheral foreland basin rocks which have greater affinity

597   to the arc and Asian plate, and the modern day Indus at the range front at Attock.

598   The variation in zircon U-Pb age spectra, and also in εNa values, between the onshore and offshore

599   downstream palaeo-Indus, and between the Eastern and Western Indus Fan (SI Figs. S1 and S3) is

600   intriguing. It could be the result of a number of factors, for example differences in sample preparation

601   procedures between operators, downstream influence of hydraulics, or additional material contributing

602   downstream, for example.

603   *5.2. Interpretation of the Murree Formation*

604   Compared to the other peripheral foreland basin sediments sampled, the Zircon U-Pb data show

605   significantly higher proportions of old grains in the Murree Formation at MHS, Kotli, and at Balakot and

606   Muzaffarabad in the HKS, but not at Paras north of Balakot (Fig. 3B, SI Fig S2, Table 1). Where

607   accompanying Sr-Nd data are available (MHS and Paras only), there is a corresponding change to more

608   negative ε_{Nd} values at MHS (Fig 2A), mirroring the change noted in the zircon data. This signature

609   indicates a higher proportion of material derived from the Indian plate (see also SI Fig S3). These

610   deposits may be interpreted as the palaeo-Jhelum Punjab tributary, which has a similar zircon U-Pb

611   spectrum to the Murree Formation (Fig. 3B), and a drainage basin consisting predominantly of the

612   Indian plate (Fig 1C). The spatial distribution of our analysed samples is consistent with this

613   interpretation: a Himalayan-derived palaeo-Jhelum type signature is prevalent in Murree Formation

614   samples at Muzaffarabad (Fig 1B) located on the modern day Jhelum River, at MHS downstream and ca

615 10 miles to the west of the modern Jhelum River, and at Kotli, downstream and 20 kms east of the

616 modern Jhelum river. It is also prevalent at Balakot, ca 15 miles upstream of the modern Jhelum River,

617 which we suggest could have been in the flood plain of the palaeo-Jhelum. 5 miles further north still,

618 near Paras, the signature is more arc-like and in this palaeo-drainage scenario, we propose lies outwith

619 the floodplain of the palaeo-Jhelum. We note that at Muzaffarabad only, through which the modern

620 Jhelum River flows, a palaeo-Jhelum type signature is also recorded, in some samples, in the underlying

621 Eocene Kuldana Formation. This may reflect the early initiation of this river, insufficiently large in its

622 early evolution to affect the downstream.

623 Alternatively, the anomalous signature from the Murree Formation compared to the rest of the

624 Cenozoic sediments in the peripheral foreland basin may reflect increased input from the Himalaya

625 attributable to a pulse of exhumation recorded in the Himalaya in the early Miocene (section 2.1.2). A

626 coeval change to greater input from the Indian plate is also recorded in the Indus Fan (Feng et al., 2021)

627 and Kirthar Ranges (Zhuang et al., 2015), supporting this interpretation. Further analyses from Murree

628 Formation samples distal to the Jhelum River should distinguish between these two alternative

629 hypotheses.

630 The difference in Murree signature compared to the rest of the foreland basin cannot be ascribed to

631 bias associated with grain size variation since the difference is reflected in both bulk rock Sr-Nd and

632 zircon proxies. Nor is there any reason to consider that a potential difference in the degree of diagenesis

633 caused the difference, since zircons are largely unaffected by this process.

634 ***5.3 What caused the change in the geochemical signature of the Indus Fan at 5-6 Ma?***

635 The more recently proposed alternatives to drainage reorganisation (Clift and Blusztajn, 2005) to

636 explain the geochemical shift in the Indus Fan at 5-6 Ma all involve tectonic explanations, namely

637 variations in exhumation of the hinterland terranes, although the extent to which increased exhumation

638   of the Lesser Himalaya versus Greater Himalaya versus Karakoram is responsible, is debated (Chirouze et

639   al 2015, Clift et al 2019, Zhou et al. 2022). Changes in monsoonal intensification are not thought to have

640   been a major influence (Clift et al., 2019, Zhou et al 2022).

641   To what extent do our data support a tectonic explanation? We focus on the peripheral foreland, which

642   should provide the most tectonically- influenced archive, above any downstream influence from the

643   Punjabi tributary system. We compare our data from the Nagri Formation (11-8.5 Ma; Table 1) to

644   modern day Indus data at the range front, this time period encompassing the 5-6 Ma date over which

645   the geochemical shift in the Indus Fan occurred.

646   The average εNd value of the two samples from the Nagri Formation is -9.65. No data are available for

647   the modern Indus at the range front. The spatially closest sample is from Besham, just south of the MCT

648   (Fig. 1C). This sample has a value of -10.7, and we would expect a more negative value by the time the

649   river had crossed to the range front, having flowed over more of the Greater Himalaya and most

650   negative Lesser Himalaya (Table 1). Thus, the shift to more negative εNd values between the Nagri

651   Formation and the estimated value for the range front in modern times I shows that variation in upland

652   tectonics over this time period could have resulted in the shift to more negative εNd values seen in the

653   Indus Fan over this time period.

654   Assignment of zircon U-Pb age populations to distinct provenances is challenging with respect to overlap

655   of the older Karakoram and Indian plate grains. Nevertheless, the 1500-2300 Ma population is typical of

656   the Lesser Himalaya. This population makes up 3% of the Nagri sample. There is no sample from the

657   modern Indus River at the range front. However, there is a sample from upstream at Attock (Fig. 1C).

658   This sample has an 11% contribution from the 1500-2300 Ma population, and we would predict a higher

659   proportion of that population after the river has flowed over a greater proportion of Indian plate

660   material. The shift to a higher proportion of zircons with ages indicative of Lesser Himalayan input

661   between the Nagri Formation and the modern day (Fig 3(, therefore supports our observations from the

662   Sm-Nd data, that upstream variations in tectonics could have resulted in the geochemical shift in the

663   Indus Fan.

664   There are no modern river mica ^{40}Ar/^{39}Ar data from the range front. Modern river ^{40}Ar/^{39}Ar mica data

665   from the trunk Indus at its river mouth at Thatta shows Plio-Pleistocene grains (1-5 Ma) indicative of

666   rapid exhumation (Clift et al., 2004). Recording of these young grains in the trunk river but not in the

667   tributaries draining only the Indian plate or Indian plate plus Hindu Kush (Clift et al., 2004; Najman et al.,

668   2009; Zhuang et al., 2018) is consistent with the viewpoints of, for example, Chirouze et al. (2015) and

669   Clift et al. (2022) Clift et al (2022), that the Karakoram and/or the Nanga Parbat syntaxis supplied this

670   young material. Lag times determined from mica data from the Neogene peripheral foreland basin

671   sedimentary rocks show no clear indication of rapid exhumation of the micas' source region after 14-16

672   Ma (Fig. 4) although n values are small and therefore populations may have been missed. Therefore a

673   period of rapid exhumation occurred sometime between Nagri Formation times and present day,

674   consistent with the view that changing exhumation in the hinterland was responsible for the

675   geochemical shift at 5 Ma in the Indus Fan.

676

677   **6.   Conclusions**

678   When the lower Indus River broadly attained its current drainage configuration, in particular when the

679   Punjab tributary system joined the main trunk river, is undocumented. Comparison of ε_{Nd} bulk rock data

680   and detrital zircon U-Pb data from Cenozoic paleo-Indus sedimentary rocks both upstream and

681   downstream of the confluence of the Indus with the Punjab tributary system shows that throughout the

682   Neogene, greater proportions of Indian plate material are recorded in the downstream compared to the

683 upstream repositories. We therefore conclude that the Punjabi tributary system, which transports

684 predominantly Indian plate detritus, had joined the trunk Indus River prior to the Neogene.

685 Whilst provenance indicators show that the proportion of Indian plate material remains constant from

686 Eocene to Neogene in the palaeo-Indus repository upstream of the confluence, the proportion of Indian

687 plate material increases in the downstream repositories, at the Eocene-Oligocene boundary in the

688 palaeo-delta, and in the mid Eocene in the Indus Fan. More research is required to understand the

689 reasons for this discrepancy in timing of the shift in the downstream repositories, but nevertheless we

690 can conclude that the Punjabi tributary system joined the palaeo-Indus trunk river at or before the start

691 of the Oligocene.

692 **Acknowledgements**

698 **Figures**

699 **Figure 1: A:** Map showing modern drainage of the Indus River with the Punjab tributary system, and the

700 Indus Fan (black dotted line). Also shown are the onshore lower Indus (Kirthar and Sulaiman) and

701 offshore IODP, ODP and DSDP locations of previously published data (Roddaz et al. 2011, Zhuang et al

702 2015, Clift et al. (2001), Clift and Blusztajn (2005), Clift et al. (2019) and Feng et al (2021). with which we

703 compare our new upstream data. Black rectangle shows the location of Fig 1B. **B:** locations of new data

704 (this study) and various towns and published sample sites discussed in text. MHS = Murree Hill Station;

705   HKS = Hazara-Kashmir Syntaxis. Samples with prefix KG96 or 99 are from Paras in the HKS, prefix MU96

706   are from Murree Hill Station, and prefix KMSr, CHSr, and NgSr are from Chinji village area. **C:** Drainage

707   superimposed on regional geology (from Clift et al., 2019). ISZ = Indus Suture zone, SSZ = Shyok Suture

708   Zone, MCT =Main Central Thrust, MBT=Main Boundary Thrust, MFT = Main Frontal Thrust.

709   **Figure 2:** ε_{Nd} values from the upstream peripheral foreland basin in Pakistan (A), and downstream Lower

710   Indus axial basin and Indus Fan (B) through time. In A, numbers adjacent to squares refer to sample

711   numbers to left. Asterisks indicate new data. Open squares for modern Indus River at Besham and

712   Thatta; hexagons are from the modern Punjabi tributaries (data from Clift et al 2002, Alizai et al. 2011,

713   Chirouze et al 2015). In B: diamonds – data from the Sulaiman and Kirthar regions of the Lower Indus

714   axial basin (Roddaz et al, 2011, Zhuang et al 2015); circles – data from the Indus Fan from Clift et al.

715   (2001), Clift and Blusztajn (2005), Clift et al. (2019), Zhou et al 2021, and Feng et al (2021). Questions

716   marks next to three Mid Eocene samples represent uncertainties in age for those samples, as depicted in

717   the original publication of Clift et al (2001). HKS = Hazara-Kashmir Syntaxis; MHS = Murree Hill Station.

718   MDA = maximum depositional age as determined from detrital grain ages (sections 2.2.1, 4.2 and 4.3).

719   Grey horizontal shading between plots A and B denote roughly equivalent time periods.

720   **Figure 3:** Detrital zircon U-Pb data shown as cumulative age distribution plots. **A**: Pakistan peripheral

721   foreland basin data excluding Murree Formation data except our new data. Kuldana Fm samples are

722   Early-Mid Eocene, Murree Formation samples are Early Miocene, Kamlial Fm is Early-Mid Miocene,

723   Chinji Fm is Mid Miocene, Nagri Fm is Late Miocene (Table 1). A inset: modern river data comparing the

724   Indus at the range front at Attock, with rivers of the Punjabi tributary system. **B:** all Murree Formation

725   data, both new and published, with comparison to the Jhelum modern river data. Murree Formation is

726   Early Miocene. **C:** comparison between peripheral foreland basin data and downstream Lower Indus

727   axial basin data and (inset) Indus Fan data. Eocene peripheral foreland basin data are omitted from the

728   figure as there are no comparative data from the downstream repositories. HKS = Hazara-Kashmir

729   Syntaxis, MHS = Murree Hill Station. All new data are asterisked. Samples with superscripts are

730   published data, as follows: [1]Ding et al (2016), [2]Qasim et al (2018), [3]Awais et al (2021), [4]Zhuang et al

731   (2015), [5]Clift et al (2002), , [6]Clift et al (2004), [7]Clift et al (2019), [8] (Zhou et al, 2021), [9]Feng et al (2021),

732   [10]Alizai et al (2011).

733   **Figure 4:** Ar-Ar mica data plotted against depositional age for new (asterisked) and published samples.

734   Note: [1]Published data from [1]Clift et al (2004) for modern Indus River data at Thatta, [2]published data

735   from Najman et al (2003) for lower Chinji Formation, [3]published data from Najman et al (2003) for the

736   Kamlial Fm, and [4]published data from Najman et al (2001) for the Murree Formation at HKS. Apart from

737   the lower Chinji Formation sample, Chinji and Nagri Formation samples are not tied to the

738   magnetostratigraphically dated section (Johnson et al 1985, section 2.2.1), and therefore the

739   depositional age range of these samples is shown by the grey bars. Note that Murree Formation samples

740   are plotted on the y axis at the age of their MDAs.

741   **Figure 5:** schematic figure showing expected and actual changes in provenance characteristics of

742   sedimentary archives upstream and downstream of the confluence, at the time when the Punjabi

743   tributary system joins the palaeo-Indus trunk river, superimposed on the modern geology. More detail

744   on analytical values summarised in this figure can be found in Table 1. Abbreviations: Av – average, Z –

745   zircon, Eoc – Eocene, KLIA – Kohistan-Ladakh Island Arc.

746   **Tables**

747   **Table 1:** comparison of provenance data from the peripheral foreland basin with those from the Lower

748   Indus Axial Basin and Indus Fan. Source region signatures also provided. Note that three "Mid Eocene"

749   data points from the Indus Fan are omitted as the age was noted as questionable in the original

750   publication of Clift et al (2001).

751 *Compiled source region data from Ahmad et al. (2000); Bignold and Treloar (2003); Clift et al. (2019);

752 DeCelles et al. (2004); DeCelles et al. (2016b); Deniel et al. (1987); Gehrels et al. (2011); Ji et al. (2009);

753 Khan et al. (1997); Khan et al. (2004); Khan et al. (2009); Mahéo et al. (2009); Miller et al. (1999);

754 Najman (2006); Pan et al. (2014); Richards et al. (2005); Robinson et al. (2001); Whittington et al. (1999);

755 Zhang et al. (2004); Zhu et al. (2012); Zhuang et al. (2018), and additional references as listed in Fig S3b.

756 **Supplementary information**

757 **Text S1**: detailed analytical methodologies and sample information

758 **Table S1**: Sr-Nd bulk mudstone data.

759 **Table S2**: detrital zircon U-Pb data.

760 **Table S3:** White mica Ar-Ar analyses.

761 **Figure SI 1:** Sr-Nd mixture modelling of end members (A), and new (asterisked) and previously published

762 bulk rock data from the peripheral and axial foreland basins in Pakistan, and the Indus Fan, plotted on to

763 a sub-region of Fig A (B). Downstream published data: [1]Roddaz et al (2011), [2]Zhuang et al (2015), [3] Clift

764 et al. (2001), Clift and Blusztajn (2005), Clift et al. (2019), Zhou et al 2021, and [4]Feng et al (2021). Means

765 and one standard errors are calculated from compiled data points (same symbols with smaller sizes and

766 transparency) (Zhuang et al., 2015 and references therein). HKS = Hazara-Kashmir Syntaxis; MHS =

767 Murree Hill Station.

768 **Figure SI 2a and b** – KDEs for new and published zircon U-Pb data, at two different scales, 0-400 Ma and

769 0-500 Ma. New data are shown by asterisks. Published data: [1]Alizai et al (2011) , [2]Clift et al (2022), [3]Ding

770 et al (2016), [4]Qasim et al (2018), [5]Awais et al (2021).

771 **Figure SI 3:** MDS plot showing zircon U-Pb data for our new samples (asterisked) from the peripheral

772 foreland basin (this study, red crosses), compared to downstream published data from the Kirthar and

773 Sulaiman ranges (purple crosses, sample prefixes SR and Z, data from Roddaz et al, 2011 and Zhuang et

774 al. 2015) and Indus Fan (data from Clift et al. 2019, Zhou et al 2021, Feng et al, 2022), grey crosses for

775 Western Fan, black crosses for Eastern Fan. Also shown are published data from the modern Indus River

776 upstream at Attock and downstream at Thatta (blue crosses, see Fig 1 for location, from Alizai et al 2011

777 and Clift et al. 2022), and end member source signatures (black hexagons for Asian plate and arc , KLA =

778 Kohistan-Ladakh Island arc, KK = Karakoram, HK = Hindu Kush, and red squares for Indian plate

779 TH=Tethyan Himalaya, GH = Greater Himalaya, LH = Lesser Himalaya. References for compiled end

780 member data are listed in Fig 3I 3b.

781 **Fig SI 4a and b** – KDEs for new and published mica Ar-Ar data from the peripheral foreland basin,

782 Pakistan, at two different scales, 0-500 Ma and 0-100 Ma. New data are asterisked, published data is

783 referenced on the plot.

784

785 **References**

786 Abbasi, I.A., Friend, P.F., 1989. Uplift and evolution of the Himalayan orogenic belts, as recorded in the
787 foredeep molasse sediments. Zeitschrift für Geomorphologie NF Supplementband 76, 75-88.
788 Ahmad, T., Harris, N., Bickle, M., Chapman, H., Bunbury, J., Prince, C., 2000. Isotopic constraints on the
789 structural relationships between the lesser Himalayan series and the high Himalayan crystalline series,
790 Garhwal Himalaya. Geological Society of America Bulletin 112, 467-477.
791 Aitchison, J.C., Ali, J.R., Davis, A.M., 2007. When and where did India and Asia collide? Journal of
792 Geophysical Research: Solid Earth (1978–2012) 112.
793 Alizai, A., Carter, A., Clift, P.D., VanLaningham, S., Williams, J.C., Kumar, R., 2011. Sediment provenance,
794 reworking and transport processes in the Indus River by U–Pb dating of detrital zircon grains. Global and
795 Planetary Change 76, 33-55.
796 Andò, S., Aharonovich, S., Hahn, A., George, S., Clift, P., Garzanti, E., 2020. Integrating heavy-mineral,
797 geochemical and biomarker analyses of Plio-Pleistocene sandy and silty turbidites: a novel approach for
798 provenance studies (Indus Fan, IODP Expedition 355). Geological Magazine 157, 929-938.
799 Argles, T., Foster, G., Whittington, A., Harris, N., George, M., 2003. Isotope studies reveal a complete
800 Himalayan section in the Nanga Parbat syntaxis. Geology 31, 1109-1112.

801   Awais, M., Qasim, M., Tanoli, J.I., Ding, L., Sattar, M., Baig, M.S., Pervaiz, S., 2021. Detrital Zircon
802   Provenance of the Cenozoic Sequence, Kotli, Northwestern Himalaya, Pakistan; Implications for India–
803   Asia Collision. Minerals 11, 1399.

804   Baig, M.S., Munir, M.-u.-H., 2007. Foraminiferal biostratigraphy of Yadgar area, Muzaffarabad Azad
805   Kashmir, Pakistan. Journal of Himalayan Earth Sciences 40.

806   Bernet, M., van der Beek, P., Pik, R., Huyghe, P., Mugnier, J.L., Labrin, E., Szulc, A., 2006. Miocene to
807   Recent exhumation of the central Himalaya determined from combined detrital zircon fission‐track
808   and U/Pb analysis of Siwalik sediments, western Nepal. Basin Research 18, 393-412.

809   Bhattacharya, G., Robinson, D.M., Wielicki, M.M., 2020. Detrital zircon provenance of the Indus Group,
810   Ladakh, NW India: Implications for the timing of the India-Asia collision and other syn-orogenic
811   processes. GSA Bulletin.

812   Bignold, S., Treloar, P., 2003. Northward subduction of the Indian Plate beneath the Kohistan island arc,
813   Pakistan Himalaya: new evidence from isotopic data. Journal of the Geological Society 160, 377-384.

814   Bossart, P., Ottiger, R., 1989. Rocks of the Murree Formation in northern Pakistan: indicators of a
815   descending foreland basin of late Paleocene to middle Eocene age. Eclogae Geologicae Helvetiae 82,
816   133-165.

817   Bouilhol, P., Jagoutz, O., Hanchar, J.M., Dudas, F.O., 2013. Dating the India–Eurasia collision through arc
818   magmatic records. Earth and Planetary Science Letters 366, 163-175.

819   Burbank, D.W., Beck, R.A., Mulder, T., 1996. The Himalayan foreland basin. The Tectonic Evolution of
820   Asia, Cambridge University Press, eds An Yin and Mark Harrison., 149-190.

821   Burbank, D.W., Tahirkheli, R.K., 1985. The magnetostratigraphy, fission-track dating, and stratigraphic
822   evolution of the Peshawar intermontane basin, northern Pakistan. Geological Society of America Bulletin
823   96, 539-552.

824   Cerveny, P., Johnson, N., 1989. Tectonic and geomorphic implications of Siwalik Group. Tectonics of the
825   Western Himalayas 232, 129.

826   Cerveny, P., Johnson, N., Tahirkheli, R., Bonis, N., 1989. Tectonic and geomorphic implications of Siwalik
827   Group heavy minerals, Tectonics of western Himalayas. Geological Society of America Special Paper 232,
828   129-136.

829   Chirouze, F., Huyghe, P., Chauvel, C., van der Beek, P., Bernet, M., Mugnier, J.-L., 2015. Stable Drainage
830   Pattern and Variable Exhumation in the Western Himalaya since the Middle Miocene. The Journal of
831   Geology 123, 1-20.

832   Clift, P., Shimizu, N., Layne, G., Blusztajn, J., Gaedicke, C., Schlüter, H.-U., Clark, M., Amjad, S., 2001a.
833   Development of the Indus Fan and its significance for the erosional history of the Western Himalaya and
834   Karakoram. Geological Society of America Bulletin 113, 1039-1051.

835   Clift, P.D., Blusztajn, J., 2005. Reorganization of the western Himalayan river system after five million
836   years ago. Nature 438, 1001-1003.

837   Clift, P.D., Campbell, I.H., Pringle, M.S., Carter, A., Zhang, X., Hodges, K.V., Khan, A.A., Allen, C.M., 2004.
838   Thermochronology of the modern Indus River bedload: New insight into the controls on the marine
839   stratigraphic record. Tectonics 23.

840   Clift, P.D., Carter, A., Jonell, T.N., 2014. U–Pb dating of detrital zircon grains in the Paleocene Stumpata
841   Formation, Tethyan Himalaya, Zanskar, India. Journal of Asian Earth Sciences 82, 80-89.

842   Clift, P.D., Carter, A., Krol, M., Kirby, E., 2002a. Constraints on India-Eurasia collision in the Arabian Sea
843   region taken from the Indus Group, Ladakh Himalaya, India. The tectonic and climatic evolution of the
844   Arabian Sea region, 97.

845   Clift, P.D., Lee, J.I., Hildebrand, P., Shimizu, N., Layne, G.D., Blusztajn, J., Blum, J.D., Garzanti, E., Khan,
846   A.A., 2002b. Nd and Pb isotope variability in the Indus River System: implications for sediment
847   provenance and crustal heterogeneity in the Western Himalaya. Earth and Planetary Science Letters
848   200, 91-106.

849   Clift, P.D., Mark, C., Alizai, A., Khan, H., Jan, M.Q., 2022. Detrital U–Pb rutile and zircon data show Indus
850   River sediment dominantly eroded from East Karakoram, not Nanga Parbat. Earth and Planetary Science
851   Letters 600, 117873.
852   Clift, P.D., Shimizu, N., Layne, G., Blusztajn, J., 2001b. Tracing patterns of unroofing in the Early Himalaya
853   through microprobe Pb isotope analysis of detrital K-feldspars in the Indus Molasse, India. Earth and
854   Planetary Science Letters 188, 475-491.
855   Clift, P.D., Zhou, P., Stockli, D.F., Blusztajn, J., 2019. Regional Pliocene exhumation of the Lesser
856   Himalaya in the Indus drainage. Solid Earth 10, 647-661.
857   Coward, M., Jan, Q., Rex, D., Tarney, J., Thirwall, M., 1984. Geology of the south Central Karakoram and
858   Kohistan, The international Karakoram project. International conference, pp. 71-85.
859   DeCelles, P., Gehrels, G., Najman, Y., Martin, A., Carter, A., Garzanti, E., 2004. Detrital geochronology
860   and geochemistry of Cretaceous–Early Miocene strata of Nepal: implications for timing and diachroneity
861   of initial Himalayan orogenesis. Earth and Planetary Science Letters 227, 313-330.
862   DeCelles, P.G., Carrapa, B., Gehrels, G.E., Chakraborty, T., Ghosh, P., 2016a. Along‐strike continuity of
863   structure, stratigraphy, and kinematic history in the Himalayan thrust belt: The view from Northeastern
864   India. Tectonics 35, 2995-3027.
865   DeCelles, P.G., Castañeda, I.S., Carrapa, B., Liu, J., Quade, J., Leary, R., Zhang, L., 2016b. Oligocene‐
866   Miocene Great Lakes in the India‐Asia Collision Zone. Basin Research.
867   DeCelles, P.G., Gehrels, G.E., Quade, J., Ojha, T., 1998. Eocene‐early Miocene foreland basin
868   development and the history of Himalayan thrusting, western and central Nepal. Tectonics 17, 741-765.
869   Deniel, C., Vidal, P., Fernandez, A., Le Fort, P., Peucat, J.-J., 1987. Isotopic study of the Manaslu granite
870   (Himalaya, Nepal): inferences on the age and source of Himalayan leucogranites. Contributions to
871   Mineralogy and Petrology 96, 78-92.
872   Ding, H., Zhang, Z., Dong, X., Tian, Z., Xiang, H., Mu, H., Gou, Z., Shui, X., Li, W., Mao, L., 2016a. Early
873   Eocene (c. 50 Ma) collision of the Indian and Asian continents: Constraints from the North Himalayan
874   metamorphic rocks, southeastern Tibet. Earth and Planetary Science Letters 435, 64-73.
875   Ding, L., Qasim, M., Jadoon, I.A., Khan, M.A., Xu, Q., Cai, F., Wang, H., Baral, U., Yue, Y., 2016b. The
876   India–Asia collision in north Pakistan: Insight from the U–Pb detrital zircon provenance of Cenozoic
877   foreland basin. Earth and Planetary Science Letters 455, 49-61.
878   DiPietro, J., Hussain, A., Ahmad, I., Khan, M.A., 2000. The main mantle thrust in Pakistan: its character
879   and extent. Geological Society, London, Special Publications 170, 375-393.
880   DiPietro, J.A., Ahmad, I., Hussain, A., 2008. Cenozoic kinematic history of the Kohistan fault in the
881   Pakistan Himalaya. Geological Society of America Bulletin 120, 1428-1440.
882   DiPietro, J.A., Pogue, K.R., 2004. Tectonostratigraphic subdivisions of the Himalaya: A view from the
883   west. Tectonics 23.
884   DiPietro, J.A., Pullen, A., Krol, M.A., 2021. Geologic history and thermal evolution in the hinterland
885   region, western Himalaya, Pakistan. Earth-Science Reviews 223, 103817.
886   Dunlap, W.J., Weinberg, R.F., Searle, M.P., 1998. Karakoram fault zone rocks cool in two phases. Journal
887   of the Geological Society 155, 903-912.
888   Exnicios, E.M., Carter, A., Najman, Y., Clift, P.D., 2022. Late Miocene unroofing of the Inner Lesser
889   Himalaya recorded in the NW Himalaya foreland basin. Basin Research 34, 1894-1916.
890   Feng, H., Lu, H., Carrapa, B., Zhang, H., Chen, J., Wang, Y., Clift, P.D., 2021. Erosion of the Himalaya-
891   Karakoram recorded by Indus Fan deposits since the Oligocene. Geology.
892   Fraser, J.E., Searle, M.P., Parrish, R.R., Noble, S.R., 2001. Chronology of deformation, metamorphism,
893   and magmatism in the southern Karakoram Mountains. Geological Society of America Bulletin 113,
894   1443-1455.
895   Gaetani, M., Garzanti, E., 1991. Multicyclic history of the Northern India continental margin
896   (Northwestern Himalaya)(1). AAPG Bulletin 75, 1427-1446.

897 Gaetani, M., Jadoul, F., Erba, E., Garzanti, E., 1993. Jurassic and Cretaceous orogenic events in the North
898 Karakoram: age constraints from sedimentary rocks. Geological Society, London, Special Publications 74,
899 39-52.
900 Garzanti, E., Andò, S., 2019. Heavy minerals for junior woodchucks. Minerals 9, 148.
901 Garzanti, E., Andò, S., Vezzoli, G., 2009. Grain-size dependence of sediment composition and
902 environmental bias in provenance studies. Earth and Planetary Science Letters 277, 422-432.
903 Garzanti, E., Andò, S., Vezzoli, G., 2020. Provenance of cenozoic indus fan sediments (IODP Sites U1456
904 and U1457). Journal of Sedimentary Research 90, 1114-1127.
905 Gehrels, G., Kapp, P., DeCelles, P., Pullen, A., Blakey, R., Weislogel, A., Ding, L., Guynn, J., Martin, A.,
906 McQuarrie, N., 2011. Detrital zircon geochronology of pre‐Tertiary strata in the Tibetan‐Himalayan
907 orogen. Tectonics 30.
908 Henderson, A.L., Najman, Y., Parrish, R., BouDagher‐Fadel, M., Barford, D., Garzanti, E., Andò, S., 2010.
909 Geology of the Cenozoic Indus Basin sedimentary rocks: Paleoenvironmental interpretation of
910 sedimentation from the western Himalaya during the early phases of India‐Eurasia collision. Tectonics
911 29.
912 Henderson, A.L., Najman, Y., Parrish, R., Mark, D.F., Foster, G.L., 2011. Constraints to the timing of India–
913 Eurasia collision; a re-evaluation of evidence from the Indus Basin sedimentary rocks of the Indus–
914 Tsangpo Suture Zone, Ladakh, India. Earth-Science Reviews 106, 265-292.
915 Hildebrand, P., Noble, S., Searle, M., Parrish, R., 1998. Tectonic significance of 24 Ma crustal melting in
916 the eastern Hindu Kush, Pakistan. Geology 26, 871-874.
917 Hildebrand, P., Noble, S., Searle, M., Waters, D., Parrish, R., 2001. Old origin for an active mountain
918 range: Geology and geochronology of the eastern Hindu Kush, Pakistan. Geological Society of America
919 Bulletin 113, 625-639.
920 Hodges, K.V., 2000. Tectonics of the Himalaya and southern Tibet from two perspectives. Geological
921 Society of America Bulletin 112, 324-350.
922 Hu, X., Garzanti, E., Wang, J., Huang, W., An, W., Webb, A., 2016. The timing of India-Asia collision
923 onset–Facts, theories, controversies. Earth-Science Reviews 160, 264-299.
924 Ji, W., Wu, F., Liu, C., Chung, S., 2009. Geochronology and petrogenesis of granitic rocks in Gangdese
925 batholith, southern Tibet. Science in China Series D: Earth Sciences 52, 1240-1261.
926 Johnson, N.M., Stix, J., Tauxe, L., Cerveny, P.F., Tahirkheli, R.A., 1985. Paleomagnetic chronology, fluvial
927 processes, and tectonic implications of the Siwalik deposits near Chinji Village, Pakistan. The Journal of
928 Geology, 27-40.
929 Jonell, T.N., Li, Y., Blusztajn, J., Giosan, L., Clift, P.D., 2018. Signal or noise? Isolating grain size effects on
930 Nd and Sr isotope variability in Indus delta sediment provenance. Chemical Geology 485, 56-73.
931 Khan, M.A., STERN, R.J., GRIBBLE, R.F., WINDLEY, B.F., 1997. Geochemical and isotopic constraints on
932 subduction polarity, magma sources, and palaeogeography of the Kohistan intra-oceanic arc, northern
933 Pakistan Himalaya. Journal of the Geological Society 154, 935-946.
934 Khan, S., Stern, R., Manton, M., Copeland, P., Kimura, J., Khan, M., 2004. Age, geochemical and Sr–Nd–
935 Pb isotopic constraints for mantle source characteristics and petrogenesis of Teru Volcanics, Northern
936 Kohistan Terrane, Pakistan. Tectonophysics 393, 263-280.
937 Khan, S.D., Walker, D.J., Hall, S.A., Burke, K.C., Shah, M.T., Stockli, L., 2009. Did the Kohistan-Ladakh
938 island arc collide first with India? Geological Society of America Bulletin 121, 366-384.
939 Koppers, A.A., 2002. ArArCALC—software for 40 Ar/39 Ar age calculations. Computers & Geosciences 28,
940 605-619.
941 Leier, A.L., Kapp, P., Gehrels, G.E., DeCelles, P.G., 2007. Detrital zircon geochronology of Carboniferous–
942 Cretaceous strata in the Lhasa terrane, Southern Tibet. Basin Research 19, 361-378.

Mahéo, G., Blichert-Toft, J., Pin, C., Guillot, S., Pêcher, A., 2009. Partial melting of mantle and crustal sources beneath South Karakorum, Pakistan: implications for the Miocene geodynamic evolution of the India–Asia convergence zone. Journal of Petrology 50, 427-449.

Malusà, M.G., Resentini, A., Garzanti, E., 2016. Hydraulic sorting and mineral fertility bias in detrital geochronology. Gondwana Research 31, 1-19.

Miller, C., Schuster, R., Klötzli, U., Frank, W., Purtscheller, F., 1999. Post-collisional potassic and ultrapotassic magmatism in SW Tibet: geochemical and Sr–Nd–Pb–O isotopic constraints for mantle source characteristics and petrogenesis. Journal of Petrology 40, 1399-1424.

Najman, Y., 2006. The detrital record of orogenesis: A review of approaches and techniques used in the Himalayan sedimentary basins. Earth-Science Reviews 74, 1-72.

Najman, Y., Bickle, M., Garzanti, E., Pringle, M., Barfod, D., Brozovic, N., Burbank, D., Ando, S., 2009. Reconstructing the exhumation history of the Lesser Himalaya, NW India, from a multitechnique provenance study of the foreland basin Siwalik Group. Tectonics 28.

Najman, Y., Garzanti, E., Pringle, M., Bickle, M., Stix, J., Khan, I., 2003. Early-Middle Miocene paleodrainage and tectonics in the Pakistan Himalaya. Geological Society of America Bulletin 115, 1265-1277.

Najman, Y., Pringle, M., Godin, L., Oliver, G., 2001. Dating of the oldest continental sediments from the Himalayan foreland basin. Nature 410, 194-197.

Najman, Y., Pringle, M., Godin, L., Oliver, G., 2002. A reinterpretation of the Balakot Formation: Implications for the tectonics of the NW Himalaya, Pakistan. Tectonics 21, 9-1-9-18.

Nyberg, B., Helland-Hansen, W., Gawthorpe, R.L., Sandbakken, P., Eide, C.H., Sømme, T., Hadler-Jacobsen, F., Leiknes, S., 2018. Revisiting morphological relationships of modern source-to-sink segments as a first-order approach to scale ancient sedimentary systems. Sedimentary Geology 373, 111-133.

Palin, R., Searle, M., Waters, D., Horstwood, M., Parrish, R., 2012. Combined thermobarometry and geochronology of peraluminous metapelites from the Karakoram metamorphic complex, North Pakistan; New insight into the tectonothermal evolution of the Baltoro and Hunza Valley regions. Journal of Metamorphic Geology 30, 793-820.

Pan, F.-B., Zhang, H.-F., Xu, W.-C., Guo, L., Wang, S., Luo, B.-j., 2014. U–Pb zircon chronology, geochemical and Sr–Nd isotopic composition of Mesozoic–Cenozoic granitoids in the SE Lhasa terrane: Petrogenesis and tectonic implications. Lithos 192, 142-157.

Pivnik, D.A., Wells, N.A., 1996. The transition from Tethys to the Himalaya as recorded in northwest Pakistan. Geological Society of America Bulletin 108, 1295-1313.

Qasim, M., Ding, L., Khan, M.A., Jadoon, I.A., Haneef, M., Baral, U., Cai, F., Wang, H., Yue, Y., 2018. Tectonic implications of detrital zircon ages from lesser Himalayan Mesozoic‐Cenozoic strata, Pakistan. Geochemistry, Geophysics, Geosystems 19, 1636-1659.

Qayyum, M., Niem, A.R., Lawrence, R.D., 2001. Detrital modes and provenance of the Paleogene Khojak Formation in Pakistan: Implications for early Himalayan orogeny and unroofing. Geological Society of America Bulletin 113, 320-332.

Richards, A., Argles, T., Harris, N., Parrish, R., Ahmad, T., Darbyshire, F., Draganits, E., 2005. Himalayan architecture constrained by isotopic tracers from clastic sediments. Earth and Planetary Science Letters 236, 773-796.

Robinson, D.M., DeCelles, P.G., Patchett, P.J., Garzione, C.N., 2001. The kinematic evolution of the Nepalese Himalaya interpreted from Nd isotopes. Earth and Planetary Science Letters 192, 507-521.

Roddaz, M., Said, A., Guillot, S., Antoine, P.-O., Montel, J.-M., Martin, F., Darrozes, J., 2011. Provenance of Cenozoic sedimentary rocks from the Sulaiman fold and thrust belt, Pakistan: implications for the palaeogeography of the Indus drainage system. Journal of the Geological Society 168, 499-516.

990 Schaltegger, U., Zeilinger, G., Frank, M., Burg, J.P., 2002. Multiple mantle sources during island arc
991 magmatism: U–Pb and Hf isotopic evidence from the Kohistan arc complex, Pakistan. Terra Nova 14,
992 461-468.
993 Schärer, U., Hamet, J., Allègre, C.J., 1984. The Transhimalaya (Gangdese) plutonism in the Ladakh region:
994 a U Pb and Rb Sr study. Earth and Planetary Science Letters 67, 327-339.
995 Schneider, D., Zeitler, P., Kidd, W., Edwards, M., 2001. Geochronologic constraints on the tectonic
996 evolution and exhumation of Nanga Parbat, western Himalaya syntaxis, revisited. The Journal of Geology
997 109, 563-583.
998 Searle, M., Khan, M.A., Fraser, J., Gough, S., Jan, M.Q., 1999. The tectonic evolution of the Kohistan‐
999 Karakoram collision belt along the Karakoram Highway transect, north Pakistan. Tectonics 18, 929-949.
1000 Searle, M., Parrish, R.R., Thow, A., Noble, S., Phillips, R., Waters, D., 2010. Anatomy, age and evolution of
1001 a collisional mountain belt: the Baltoro granite batholith and Karakoram Metamorphic Complex,
1002 Pakistani Karakoram. Journal of the Geological Society 167, 183-202.
1003 Shah, S.I., 2009. Stratigraphy of Pakistan. Government of Pakistan Ministry of Petroleum & Natural
1004 Resorces Geological Survey of Pakistan.
1005 Sinclair, H., Jaffey, N., 2001. Sedimentology of the Indus Group, Ladakh, northern India: implications for
1006 the timing of initiation of the palaeo-Indus River. Journal of the Geological Society 158, 151-162.
1007 Treloar, P., Rex, D., Guise, P., Wheeler, J., Hurford, A., Carter, A., 2000. Geochronological constraints on
1008 the evolution of the Nanga Parbat syntaxis, Pakistan Himalaya. Geological Society, London, Special
1009 Publications 170, 137-162.
1010 Treloar, P.J., Palin, R.M., Searle, M.P., 2019. Towards resolving the metamorphic enigma of the Indian
1011 Plate in the NW Himalaya of Pakistan. Geological Society, London, Special Publications 483, 255-279.
1012 Ullah, K., Arif, M., Shah, M.T., 2015. Geochemistry and provenance of the Lower Siwaliks from
1013 southwestern Kohat, western Himalayan Foreland Basin, NW Pakistan. Geologica Acta: an international
1014 earth science journal 13, 45-61.
1015 Van Der Beek, P., Van Melle, J., Guillot, S., Pêcher, A., Reiners, P.W., Nicolescu, S., Latif, M., 2009. Eocene
1016 Tibetan plateau remnants preserved in the northwest Himalaya. Nature Geoscience 2, 364-368.
1017 van Hinsbergen, D.J., Lippert, P.C., Dupont-Nivet, G., McQuarrie, N., Doubrovine, P.V., Spakman, W.,
1018 Torsvik, T.H., 2012. Greater India Basin hypothesis and a two-stage Cenozoic collision between India and
1019 Asia. Proceedings of the National Academy of Sciences 109, 7659-7664.
1020 Wallis, D., Carter, A., Phillips, R.J., Parsons, A.J., Searle, M.P., 2016. Spatial variation in exhumation rates
1021 across Ladakh and the Karakoram: New apatite fission track data from the Eastern Karakoram, NW India.
1022 Tectonics.
1023 Welcomme, J.-L., Benammi, M., Crochet, J.-Y., Marivaux, L., Métais, G., Antoine, P.-O., Baloch, I., 2001.
1024 Himalayan Forelands: palaeontological evidence for Oligocene detrital deposits in the Bugti Hills
1025 (Balochistan, Pakistan). Geological Magazine 138, 397-405.
1026 Whittington, A., Foster, G., Harris, N., Vance, D., Ayres, M., 1999. Lithostratigraphic correlations in the
1027 western Himalaya—an isotopic approach. Geology 27, 585-588.
1028 Willis, B., 1993. Evolution of Miocene fluvial systems in the Himalayan foredeep through a two
1029 kilometer-thick succession in northern Pakistan. Sedimentary geology 88, 77-121.
1030 Yeats, R.S., Hussain, A., 1987. Timing of structural events in the Himalayan foothills of northwestern
1031 Pakistan. Geological society of America bulletin 99, 161-176.
1032 Yu, Z., Colin, C., Wan, S., Saraswat, R., Song, L., Xu, Z., Clift, P., Lu, H., Lyle, M., Kulhanek, D., 2019. Sea
1033 level-controlled sediment transport to the eastern Arabian Sea over the past 600 kyr: Clay minerals and
1034 SrNd isotopic evidence from IODP site U1457. Quaternary Science Reviews 205, 22-34.
1035 Zaleha, M.J., 1997. Intra‐ and extrabasinal controls on fluvial deposition in the Miocene Indo‐Gangetic
1036 foreland basin, northern Pakistan. Sedimentology 44, 369-390.

1037 Zanchi, A., Gaetani, M., 2011. The geology of the Karakoram range, Pakistan: the new 1: 100,000
1038 geological map of Central-Western Karakoram. Italian journal of geosciences 130, 161-262.
1039 Zhang, H., Harris, N., Parrish, R., Kelley, S., Zhang, L., Rogers, N., Argles, T., King, J., 2004. Causes and
1040 consequences of protracted melting of the mid-crust exposed in the North Himalayan antiform. Earth
1041 and Planetary Science Letters 228, 195-212.
1042 Zhou, P., Stockli, D.F., Ireland, T., Murray, R.W., Clift, P.D., 2021. Zircon U‑Pb Age Constraints on NW
1043 Himalayan Exhumation from the Laxmi Basin, Arabian Sea. Geochemistry, Geophysics, Geosystems,
1044 e2021GC010158.
1045 Zhou, P., Stockli, D.F., Ireland, T., Murray, R.W., Clift, P.D., 2022. Zircon U‑Pb Age Constraints on NW
1046 Himalayan Exhumation from the Laxmi Basin, Arabian Sea. Geochemistry, Geophysics, Geosystems,
1047 e2021GC010158.
1048 Zhu, D.-C., Mo, X.-X., Niu, Y., Zhao, Z.-D., Wang, L.-Q., Liu, Y.-S., Wu, F.-Y., 2009. Geochemical
1049 investigation of Early Cretaceous igneous rocks along an east–west traverse throughout the central
1050 Lhasa Terrane, Tibet. Chemical Geology 268, 298-312.
1051 Zhu, D.-C., Zhao, Z.-D., Niu, Y., Dilek, Y., Wang, Q., Ji, W.-H., Dong, G.-C., Sui, Q.-L., Liu, Y.-S., Yuan, H.-L.,
1052 2012. Cambrian bimodal volcanism in the Lhasa Terrane, southern Tibet: record of an early Paleozoic
1053 Andean-type magmatic arc in the Australian proto-Tethyan margin. Chemical Geology 328, 290-308.
1054 Zhuang, G., Najman, Y., Guillot, S., Roddaz, M., Antoine, P.-O., Métais, G., Carter, A., Marivaux, L.,
1055 Solangi, S.H., 2015. Constraints on the collision and the pre-collision tectonic configuration between
1056 India and Asia from detrital geochronology, thermochronology, and geochemistry studies in the lower
1057 Indus basin, Pakistan. Earth and Planetary Science Letters 432, 363-373.
1058 Zhuang, G., Najman, Y., Tian, Y., Carter, A., Gemignani, L., Wijbrans, J., Jan, M.Q., Khan, M.A., 2018.
1059 Insights into the evolution of The Hindu Kush-Kohistan-Karakoram from modern river sand detrital geo-
1060 and thermochronological studies. Journal of the Geological Society, jgs2018-2007.

1061

Terrane/ Basin Stratigraphy	εNd	Zircons % with U-Pb ages 40-200 Ma (arc-derived)
Source region characteristics[*] (GHS, LHS, THS = Greater-, Lesser-, Tethyan Himalaya respectively; NP = Nanga Parbat)		
Karakoram	Average: -10	Dominant 40-200 Ma populations with some older grains to Precambrian
Kohistan Island arc	Average: +5	Entirely 40-200 Ma
Indian plate	Avgs: -15 (GHS), -22 (LHS & NP), -11 (THS)	Near 100% > 200 Ma.
Upstream peripheral foreland basin (new & published data of [1]Clift et al 2002, [2]Alizai et al., 2011 and Clift et al 2022, [3]Ding et al 2016, [4]Qasim et al 2018)		
Modern Indus River	*No data for downstream of GHS* [1]At Skardu (upstream of GHS) -8.6 [1]At Besham (just into GHS) -10.7	[2]At Attock: 53% arc
Upper Miocene Nagri Fm	-9.4, -9.9	67% arc
Mid Miocene Chinji Fm	-7.7, -8.7 (our data). Chirouze et al., (2015) data: -3.8 to -7.7	47% arc
L-mid Miocene Kamlial Fm	-8.3	51% arc
Lower Miocene Murree Fm	-13.8 (MHS) -8.1, -9.2 (HKS, Paras north of Balakot)	23% arc (MHS) 50% arc (HKS, Paras north of Balakot) [3]0-4% arc (HKS, Balakot) [3]0-17% (HKS Muzaffarabad)
Lower-mid Eocene Kuldana Fm	-8.1, -8.8	[3]49-75% arc (HKS, Balakot) [3]6-74% arc (HKS, Muzaffarabad) Qasim Murree Hill station [4]34-78% arc (MHS)
Downstream Lower Indus axial basin, Kirthar (K) and Sulaiman (S) regions ([1]Clift et al. 2002, [5]Clift et al. 2004, [6]Roddaz et al 2011, [7]Zhuang et al. 2015)		
Modern Indus River	-15[1] (below Sutlej confluence and at delta)	[5]At Thatta: 18% arc
Pliocene Siwalik Gp	-12 (K[7]) n=2	12% arc (K[7])
U. Miocene Siwaliks	-9.3 (K[7]) n=1	
M. Miocene Siwalik Gp & Vihowa Fm	-11 (K[7]) n=8	22% arc (K[7])
L. Miocene Vihowa & Chitarwata Fms.	-10.5 (S[6]) n=2, -13.1 (K[7]) n=5	
Upper Oligocene Chitarwata Fm	Upper upper Oligocene -11.1 (S[6]) n=3 Lower upper Oligocene -12.4 (S[6]) n=3	
Lower Oligocene Chitarwata Fm	-9.6 (S[6]) n=1; -13.4 (K[7]) n=1	16% arc (K[7)]); 16% arc (S[7)])
L-mid Eocene Ghazij & Kirthar Gps	Av.-9.3 (S[6]) n=2, -7.5 (K[7]) n=1	
Indus Fan ([8]Clift et al 2001 ; [9]Clift & Blusztajn 2005; [10]Clift et al 2019 ; [11]Feng et al. 2021 ; [12]Zhou et al. 2022).		
Pliocene	[9]Av. -10.8 (n=8)	[10, 12]19-32%
Miocene	[8,10,11]Av. -10.1 (n=47)	[10,11, 12]11-48%
Oligocene	[8, 10]Av. -11.9 (n=16)	[11]16-43%
M. Eocene	[8]-11.96, -5.2	
E. Eocene	[9]-9.3	

Figure 1Amap

Figure 1 b c

(B) Topography (m)
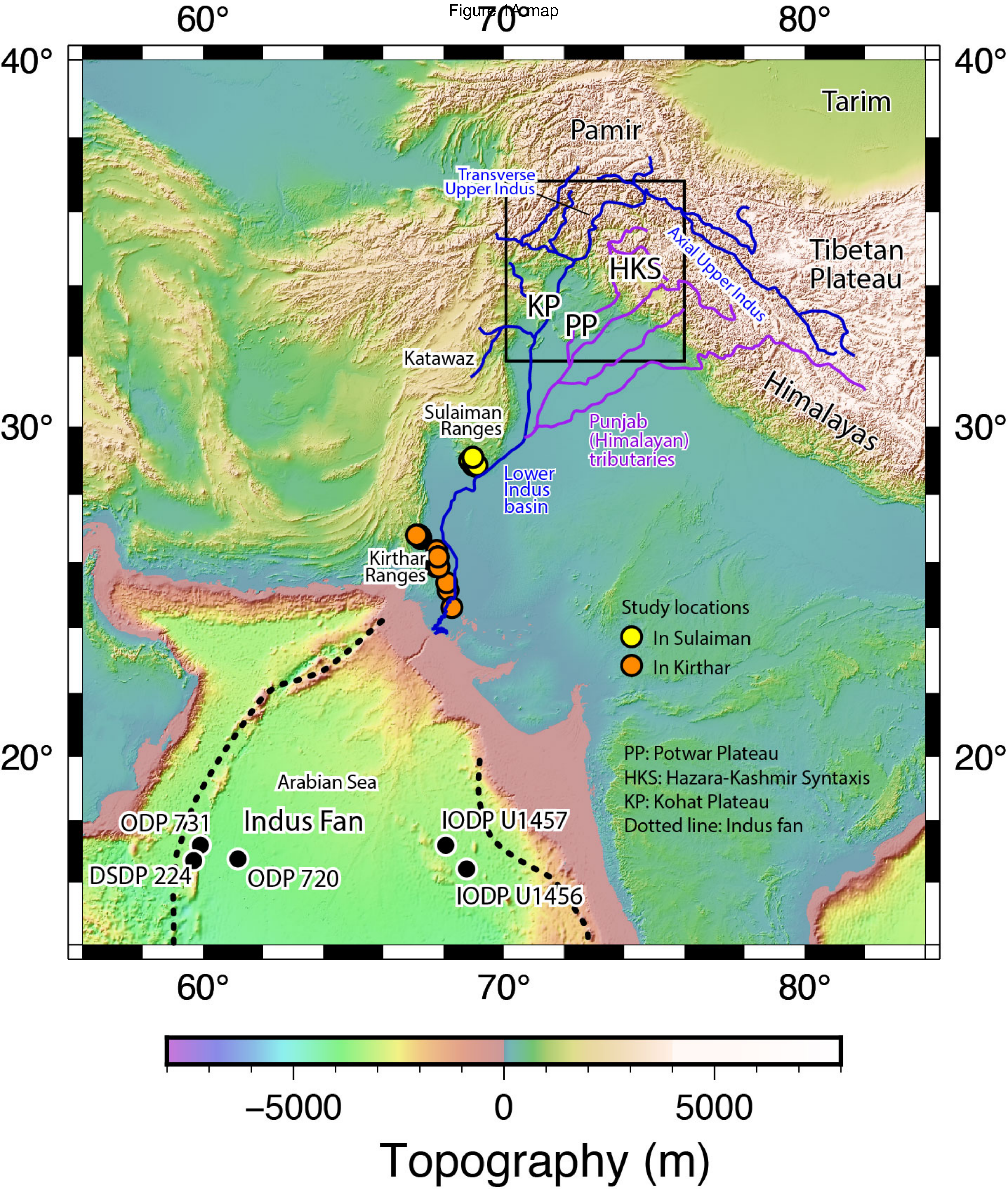
(C)
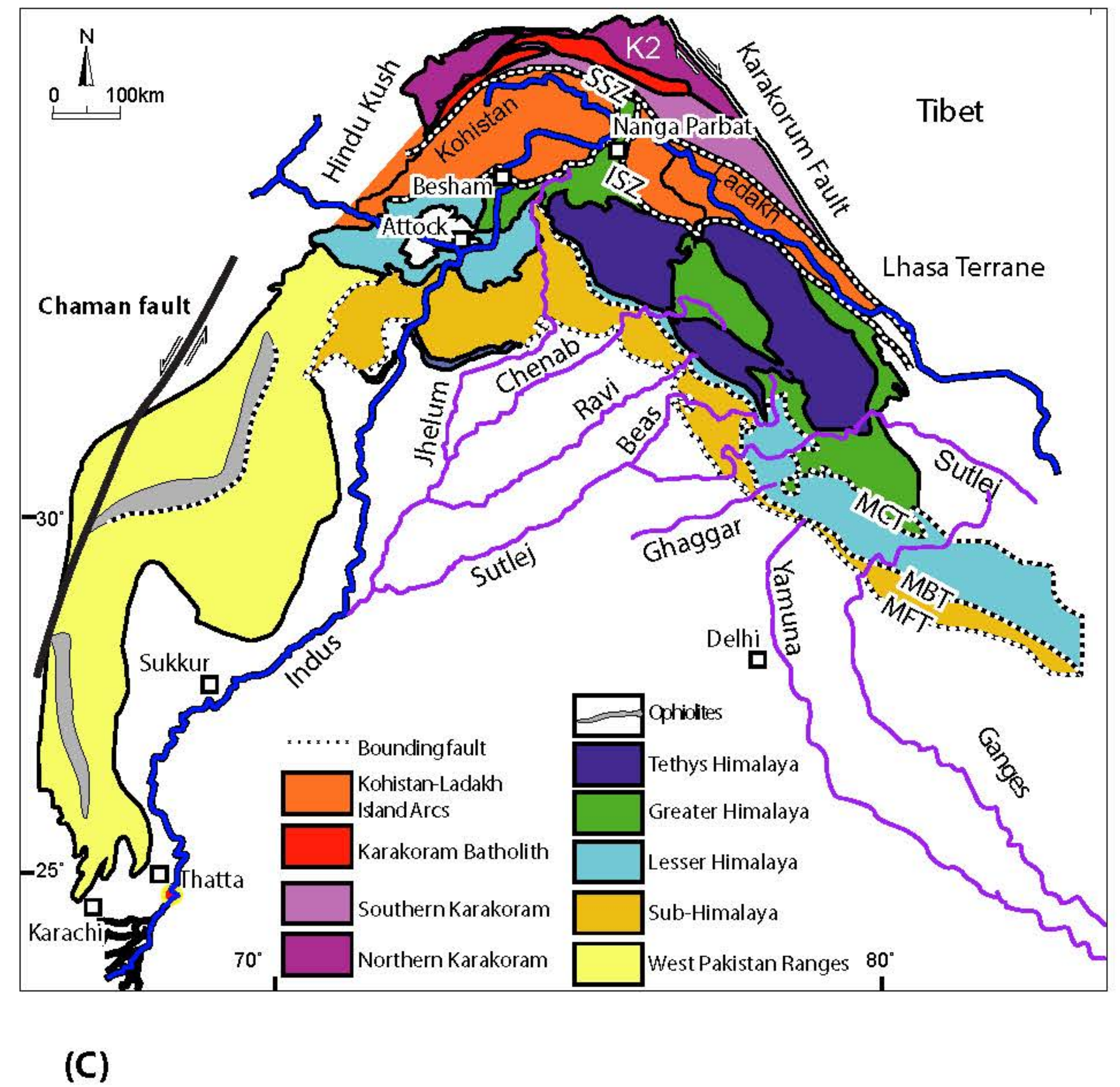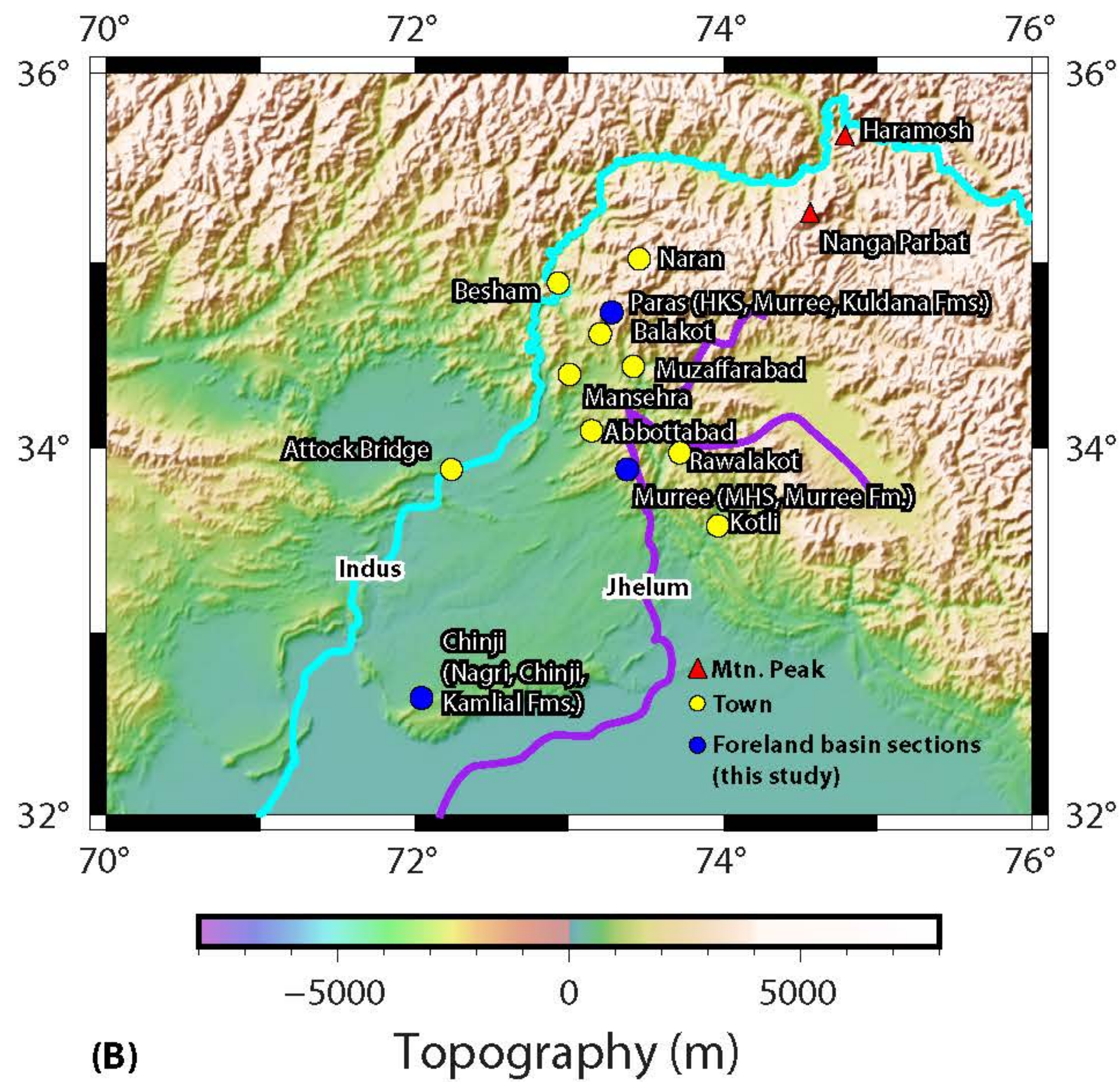
Figure 2 eps Nd against stratigraphy

(A)

modern river sediments

Indus at Thatta

Indus at Besham

Forestland basin samples mean (n = 9; this study, excluding the Murree Fm at MHS)

Age (Ma)

Sutlej   Jhelum   Chenab   Ravi

1 - NGSr-1A (Nagri Fm) *
2 - NGSr-2A (Nagri Fm) *   **11-8.5 Ma**

3 - CHSr-2A (Chinji Fm) *
4 - CHSr-1A (Chinji Fm) *   **14-11 Ma**

5 - KMSr-5A (Kamlial Fm) *   **18-14 Ma**

6 - MU96-2C (Murree Fm at MHS) *   **MDA (MHS): 24 Ma**

7 - KG96-22C (Murree Fm at HKS) *   **MDA (HKS): 23 Ma**
8 - KG96-30A (Murree Fm at HKS) *

9 - KG99-5E (Kuldana Fm) *
10 - KG99-14C (Kuldana Fm) *   **53-43 Ma**

ε_{Nd}

ε_{Nd}

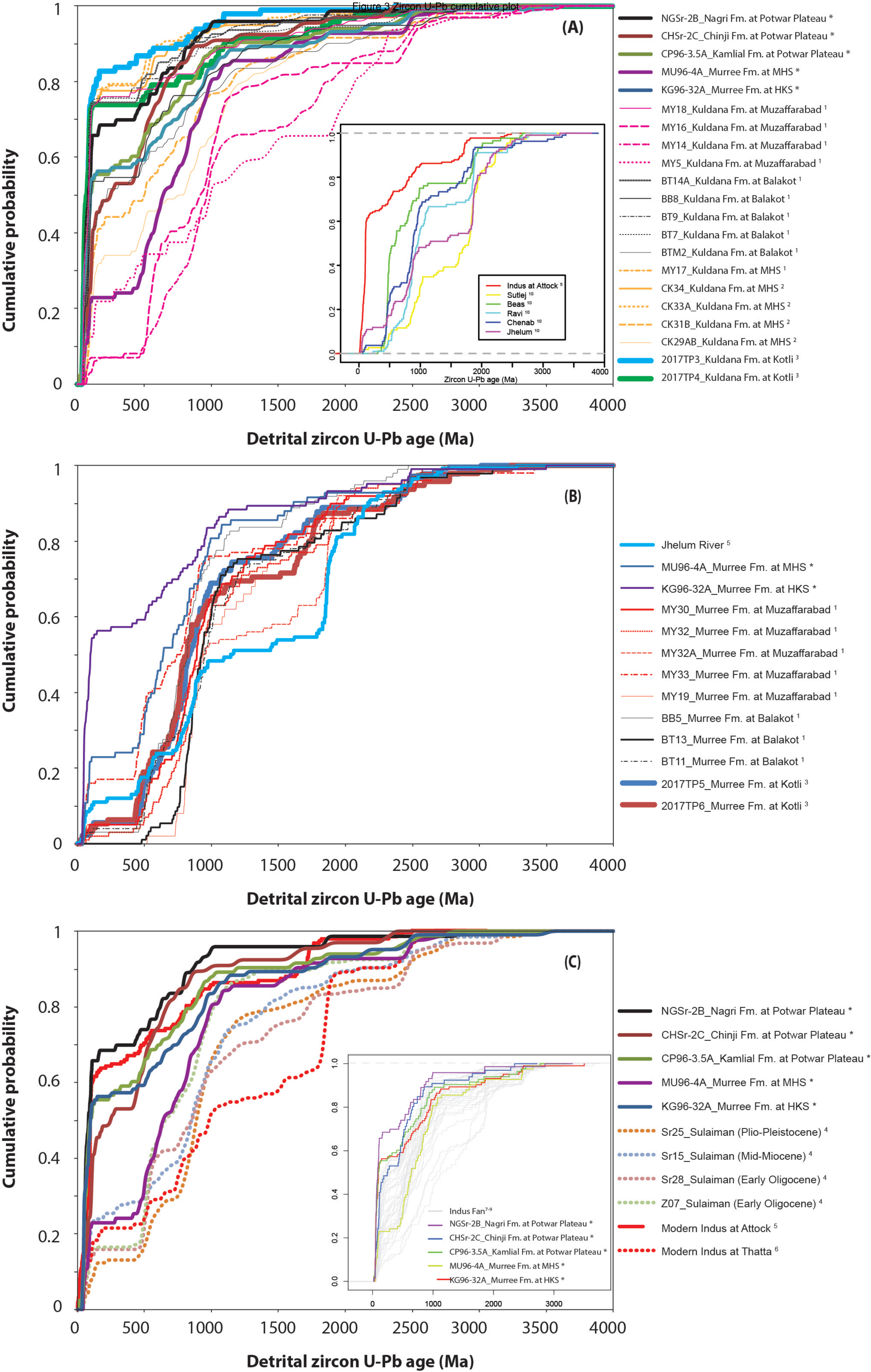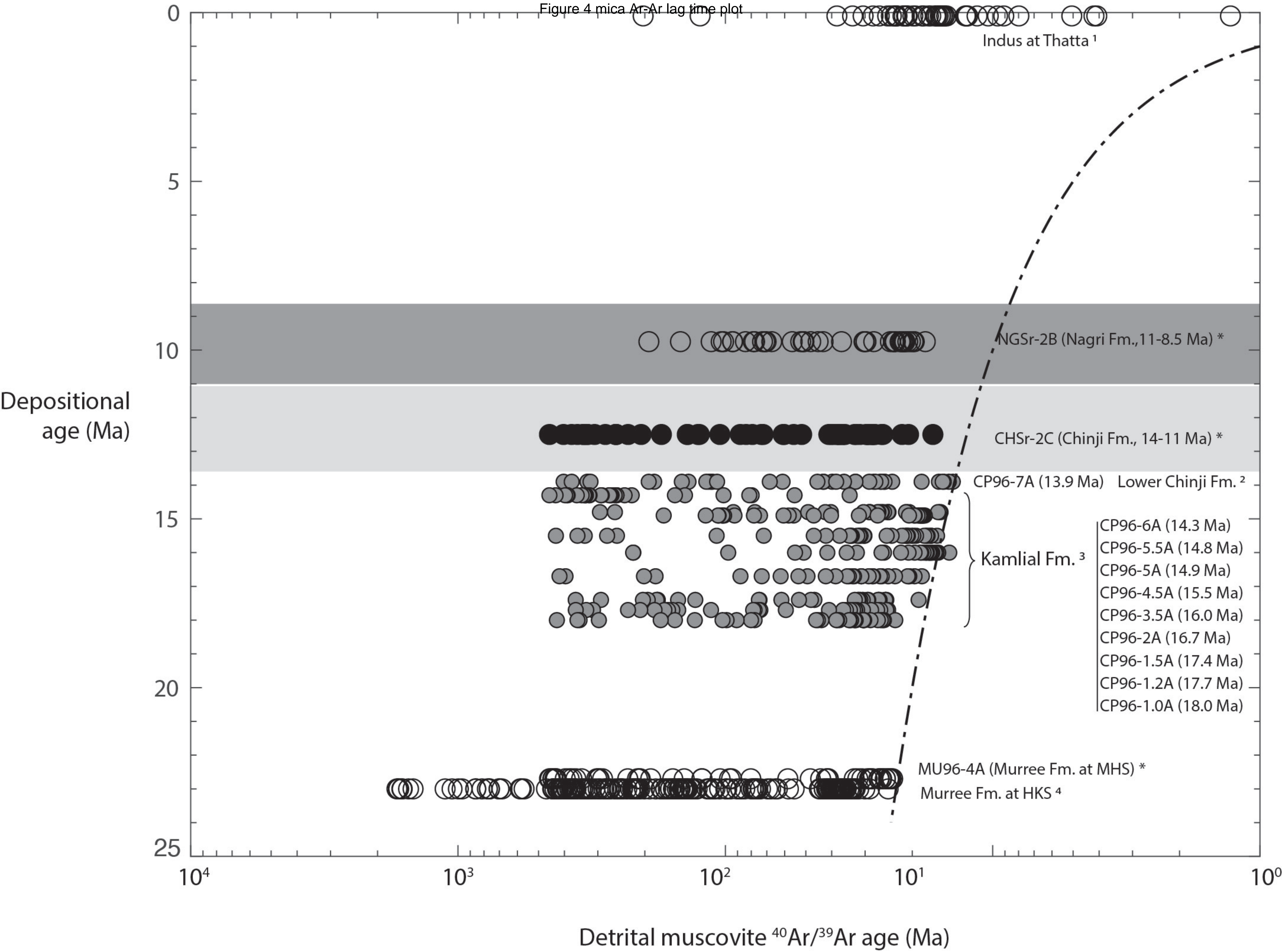Figure 3 Zircon U-Pb cumulative plot

Figure 3 Zircon U-Pb cumulative plot

Figure 4 mica Ar-Ar lag time plot

Figure 5 schematic palaeodrainage